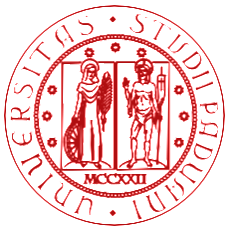

UNIVERSITÀ DEGLI STUDI DI PADOVA

TESAF

MSc In Sustainable Forest and Nature Management

Assessment of trends in rainfall-runoff events in a mountain basin: analysis of the influence of initial conditions by means of a hydrological model and GIS

Master Candidate
Deepak Kumar Yadav
Student ID: 2072331

Supervisor
Prof. Eleonora Dallan
University of Padova

Co-Supervisor
Dr. Ylenia Gelmini
Prof. Marco Borga
University of Padova

Academic Year
2022/2023

Acknowledgement

I am immensely grateful to my thesis supervisor, Professor Eleonora Dallan, for her constant motivation, guidance, and unwavering support throughout the thesis project.

I would also like to express my deep appreciation to my co-supervisor and mentor, Dr. Ylenia Gelmini, for her constant support and encouragement during every phase of my thesis. Her mentorship and belief in my abilities have been invaluable in overcoming challenges and staying focused on achieving this marvellous work.

To Professor Marco Borga, co-supervisor, and my mentor, I extend my sincere gratitude for providing me with the direction needed to navigate through the complexities of my research.

Thanks, must be given to the Bolzano province for their invaluable contribution in furnishing us with satellite observations MODIS snow cover area data in coordination with EURAC research centre. I am equally thankful to ARPAV for providing precipitation and temperature time series data.

I am indebted to my friend and mentor, Akriti Joshi, Muzamil Hussain, Harin Aiyanna, Cheriyanda Raveendra, and Brady Orozoco-Herman, for their support and mentorship.

To all my friends from different corners of the world who were part of this incredible journey, I want to thank you for making this journey unforgettable. Your camaraderie, diverse perspectives, and unwavering support have enriched my academic and personal experiences beyond measure.

I extend my gratitude to my esteemed teachers and mentors at Bangor University, UK, as well as the University of Padova, Italy. I am immensely thankful to the European Union for the Erasmus Mundus Scholarship, which played a pivotal role in realizing my aspiration to pursue international studies.

My sincere thanks to my family, my support system for their unwavering support and unconditional love: Shiv Ram Yadav, Rita Yadav, Sabita Kumari Yadav, Dr. Pappu Kumar Yadav, who always motivated and supported me in exploring more in the forestry sector and achieving this incredible feat.

Abstract

Despite the expectation that increases in rainfall with climatic change will result in increases in pluvial flooding, there is more historical evidence for decreases in flood magnitude in the La Vizza basin. The small basin of La Vizza, in the Eastern Italian Alps, provides a clear example for this type of trend divergence. In this basin, flood magnitudes are decreasing, despite increasing rainfall extremes. In this thesis we investigate how changes in soil moisture and snow water equivalent play a role in controlling the above divergence. Using catchment average precipitation and temperature, and a continuous hydrological model able to specify soil moisture and snow water equivalent at the start of each rainfall-runoff events, we aim to better understand the relative role of the two drivers in controlling the trends in runoff events. Additionally, trends in annual maxima of rainfall, annual maximum of runoff, mean annual temperature, antecedent soil moisture, and antecedent snow water equivalent are scrutinized to provide a comprehensive understanding. The study employs a hybrid approach, coupling the ICHYMOD model with the TOPMELT continuous hydrological model to simulate antecedent soil moisture and snow water equivalent. A total of 944 rainfall-runoff events were selected between 1 October 1985 to 31 September 2018 (33-year timeframe) for detailed analysis. Model outputs were compared with observed runoff at the La Vizza outlet to assess model efficiency. Additionally, satellite-based MODIS snow cover area data were incorporated for comparison using GIS analysis. The assessment of trend in antecedent soil moisture and antecedent snow water equivalent, aligned with selected events and standards, was conducted using the Mann-Kendall test and Sen slope statistical estimator. Results revealed noteworthy trends. Annual maximum of rainfall demonstrated an upward trajectory, with a maximum increase of up to 12.30% for rainfall duration of 30 minutes whereas annual maxima of runoff was decreased by -12.4% for runoff duration of 5 minutes over a ten-year period. Mean annual temperature depicted statistically significant rising trends, exhibiting an average increase of 15.19% over a decade, equivalent to a rise of 0.49° Celsius. Conversely, antecedent soil moisture and antecedent snow water equivalent indicate minor decreasing trends. The negative decreasing trend in the runoff coefficient, antecedents snow water equivalent, and antecedents soil moisture well explain the decreasing runoff peak. These results shed light on the role of antecedents' conditions on runoff process.

Table of Contents

List of Figures

List of Tables

1. Introduction

Mountain catchments are integral components of hydrological systems, playing a pivotal role in supplying water resources to downstream regions. However, they are exceptionally vulnerable to the impacts of climate change, which can significantly alter the hydrological processes governing their water supply (Moraga et al., 2021; Somers & McKenzie, 2020). Key contributors to the water supply in mountainous areas are snowmelt and rainfall, making these catchments particularly sensitive to variations in temperature and precipitation patterns (Day, 2009). The rapid transformation of high mountain regions due to global warming raises concerns about the evolution of natural hazards in these areas (Beniston et al., 2018; Musselman et al., 2017). Climate change, as a principal driver of environmental transformation, exerts profound influence on hydrological systems, particularly in alpine regions. In the Alps, atmospheric warming has been observed to more than double the global mean value over the past 50 years (Böhm et al., 2001). The intricate interplay between changing atmospheric conditions and hydrological processes underscores the need for comprehensive investigations.

Climatic shifts, coupled with varying human impacts, emerge as the primary drivers of changes in rainfall-runoff dynamics (Kliment et al., 2011). The indisputable influence of anthropogenic activities on climate change is underscored by the Intergovernmental Panel on Climate Change (IPCC) report (2013), which attributes a significant temperature increase of 0.89°C from 1901 to 2012 to human-induced factors (Umar et al., 2022). The response of streamflow to rainfall-runoff events is influenced by various factors, including the characteristics of the events themselves, such as their intensity, duration, and frequency (Guastini et al., 2019). Additionally, soil moisture content in catchments plays a crucial role in modulating the rainfall-runoff response (Bronstert & Bárdossy, 1999; Zehe et al., 2005, 2010; Zehe & Blöschl, 2004). Understanding the spatial scale-dependent variations in rainfall-runoff events holds promise in elucidating the main drivers behind the temporal variability of streamflow responses in catchments of diverse sizes (Guastini et al., 2019).

Moreover, event water contributions to streamflow have been found to be influenced by antecedent soil moisture conditions, event size, and rainfall intensity (Penna et al., 2016). This highlights the complex interplay between antecedent conditions and hydrological response. Antecedent soil moisture has emerged as a pivotal factor governing the non-linear behaviour of runoff (Brocca et

al., 2005; Penna et al., 2011; Radatz et al., 2013; Western et al., 2004; Zhao et al., 2015). The role of antecedent soil moisture, however, appears to vary when analysing different metrics of streamflow response. Although it is acknowledged as a critical driver of runoff generation in mountain catchments in various studies (Brocca et al., 2009; James & Roulet, 2009; Massari et al., 2014; Tayfur et al., 2014; Tramblay et al., 2010), its role in explaining the variability of response metrics may differ, sometimes overshadowed by event rainfall (Merz & Blöschl, 2009; Uber et al., 2018).

Trend analysis is considered to be a crucial tool in detecting and understanding the rainfall-runoff mechanics in a long-term series of hydrological and meteorological data and the outcomes from such analysis stand out promising in supporting the findings from the different forecasting hydrological model for the planning and management of water resources (Kliment et al., 2011). The assessment of trends in hydro-meteorological data offers a valuable avenue for evaluating the influence of climate change on hydrological systems (Chen & Georgakakos, 2014; Darand et al., 2015; Sa'adi et al., 2019). Projections indicate that climate change will likely induce significant hydrological alterations, leading to shifts in trends and the recurrence intervals of extreme events (Umar et al., 2022). Consequently, researchers have increasingly utilized statistical and stochastic techniques to detect trends and alterations in hydrological time series across varying temporal scales (Caloiero et al., 2011).

In recent years, amidst mounting apprehensions regarding the ramifications of climatic fluctuations (IPCC, 2007), researcher have employed a diverse array of statistical and stochastic methodologies to detect trends and transitions within hydrological datasets, across varying temporal granularities (Caloiero et al., 2011). In the domain of hydrometeorological variables, such as precipitation, nonparametric statistical tests have recurrently been enlisted to corroborate findings already perceived via more conventional analytical techniques, including moving averages and regression analysis (Bocchiola et al., 2002; Bradley, 1998; Kundzewicz & Robson, 2004).

Man-Kendall test is one of the popular method for the trend detection and is widely used in different studies for the trend detection in the hydrometeorological variables around the world (e.g. Arnbjerg-Nielsen, 2006; Bormann et al., 2011; Brázdil et al., 2012; Douglas et al., 2000; Gregersen et al., 2013; Jurko et al., 2009; Korhonen & Kuusisto, 2010; Kyselý, 2009; Madsen et al., 2009;

Meilutytė-Barauskienė et al., 2010; Petrow et al., 2009; Petrow & Merz, 2009; Sadri et al., 2009; Wilson et al., 2010 and others), renowned for its non-parametric nature, robustness, and insensitivity to outliers (Chevuturi et al., 2018; Hirsch et al., 1993; Salas & Maidment, 1993). For, this study, the trends has been assessed using the non-parametric Mann-Kendall test (Kendall, 1975; Mann, 1945) and the trend slopes has been determined by using Sen's slope method (Sen, 1968).

The scientific community has long recognized the significance of extreme precipitation events in shaping hydrological regimes. Analysing observed data, Madsen et al. (2014) reported a noticeable increase in extreme precipitation across Europe. In regions marked by snowmelt-driven peak flows, studies have documented declining trends in extreme streamflow and earlier spring snowmelt peaks, likely attributable to rising temperatures (Madsen et al., 2014). Climate projections further suggest a future marked by intensified extreme precipitation (Madsen et al., 2014), posing substantial hydrological alterations such as shifts in flood magnitudes and early spring floods in catchments with snowmelt-dominated peak flows.

Empirical studies in specific regions have provided insights into changing hydrological patterns. For instance, investigations in Northern Italy revealed an increasing trend in annual maxima of long daily rainfall series (Dallan et al., 2022; De Michele et al., 1998; Libertino et al., 2019; Montanari et al., 1996), while further analyses covering a broader timespan demonstrated varying trends in total annual rainfall, rainy days, and event intensity (Brunetti et al., 2001).

Despite the expectation that increases in rainfall with climatic change will result in increases in pluvial flooding, there is more historical evidence for decreases in flood magnitude in the La Vizza basin (Marcon, 2023). In this basin, flood magnitudes are decreasing, despite increasing rainfall extremes. In this thesis we investigate how changes in soil moisture and snow water equivalent play a role in controlling the above divergence. Using catchment average precipitation and temperature, and a continuous hydrological model able to specify soil moisture and snow water equivalent at the start of each rainfall-runoff events, we aim to better understand the relative role of the two drivers in controlling the trends in runoff events (both volumes and peaks). With this overarching objective, the thesis has the specific objectives of:

i. quantifying the diverging trends in annual maxima of rainfall and runoff events for the study basin

ii. quantifying the snow cover area by means of the TOPMELT model and validating it by using MODIS satellite images
iii. quantifying the trends for event-generating precipitation, antecedent soil moisture, and antecedent snow water equivalent and assess their role in controlling the trend in runoff events.

While there has been research on the Italian Alps region regarding how frequent heavy precipitation in the recent years (Borga et al., 2007) is determining trends runoff (Marcon, 2023), the specific role of the initial conditions of soil moisture and snow water equivalent before the events remain unexplored in the La Vizza basin. To address this gap, the integration of a hydrological models, TOPMELT and ICHYMOD, along with the GIS, has been used in this study. TOPMELT has been structured to simulate snowpack dynamics and its interplay with runoff, whereas ICHYMOD has been employed for calculating streamflow behaviours. Through this integration, the ability to analyse the influence of diverse initial conditions on runoff trends has been facilitated. By employing the hydrological model TOPMELT, which incorporates snow and glacier melt considerations, it has become possible to simulate the evolving dynamics of these processes under varying initial conditions. This is exemplified in the examination of how differing antecedent soil moisture levels impact responses related to snowmelt and runoff. The capacity of TOPMELT to compute snow water equivalents and simulate their spatial distribution aids in comprehending how distinct initial conditions govern the temporal and spatial characteristics of runoff patterns. Conversely, the ICHYMOD hydrological model encompasses a wider spectrum of runoff processes and effectively integrates the outcomes derived from TOPMELT, enabling an assessment of their collective influence on streamflow. This comprehensive evaluation contributes to an enhanced understanding of how initial conditions shape the hydrological response within the La Vizza basin.

2. Data and study area

2.1.Study area

This study centres on the small basin of La Vizza basin, which occupies a pivotal position within the Upper Cordevole River system, nestled in the eastern Italian Alps. This basin finds its geographical niche within the majestic Dolomite Mountains, an iconic feature of northern Italy's landscape. More specifically, the study area is strategically situated in the western part of the Livinallongo del Col di Lana commune, which falls under the administrative jurisdiction of the Province of Belluno within the Veneto region. A visual depiction of this geographic alignment is presented in Fig. 1, providing a cartographic snapshot of the study area's precise location.

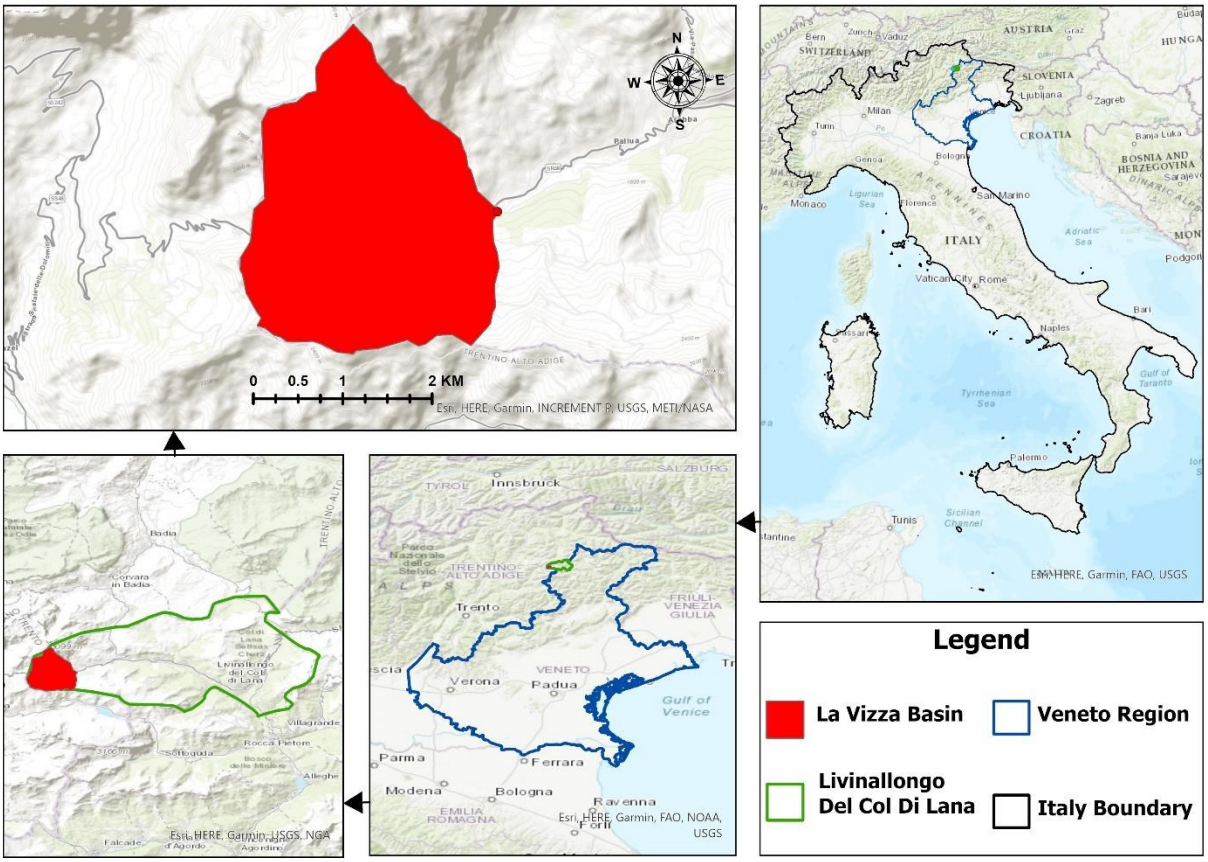

Fig 1: Location map of the study basin. Red polygons indicate the study basin.

The study basin, La Vizza encompasses a geographical area of 7.3 square kilometres, characterized by altitudes ranging from 1843 to 3152 meters above sea level (a.s.l.). The average elevation of the basin is 2342 m a.s.l., with about a quarter of the area lying above 2500 m a.s.l. In terms of climate, the basin experiences notable fluctuations in monthly average temperatures. January

marks the coldest period with an average of -5.7 °C, while July registers the warmest month with a peak of 14.1 °C.

The predominant land cover in the La Vizza basin is alpine grassland, covering approximately 74% of the total area. Shrubs account for 14% of the land cover, while rocks make up approximately 12%. The hydrological dynamics within the basin are significantly influenced by precipitation, with an average annual precipitation of 1220 mm. The bulk of this precipitation takes the form of snow during the winter months. Subsequently, the melting of this snow during the spring and summer months assumes paramount importance as it contributes significantly to the water resources of the rivers and streams that traverse the basin (Guastini et al., 2019).

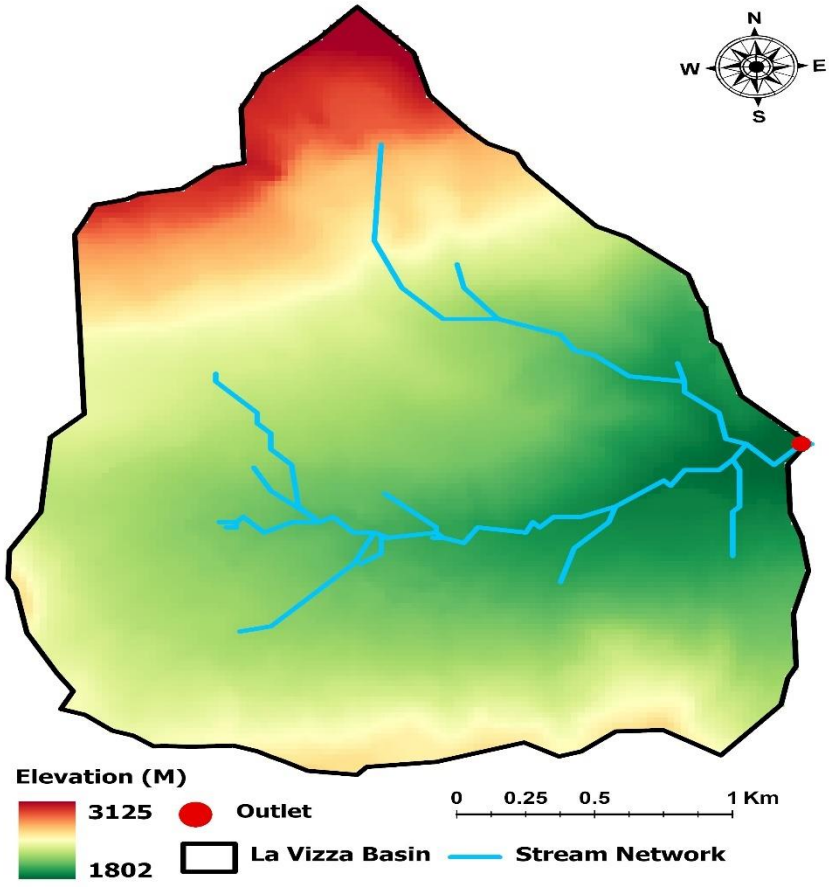

Fig 2: Elevation map of Study basin. The red dots indicate the outlet of La Vizza.

Geologically, the basin is underpinned by two primary lithological formations. The Dolomia Cassiana formation predominantly consists of dolomite, while the San Cassiano formation

comprises a combination of carbonate and terrigenous sandstones and claystones. The soils in this area exhibit a moderate depth and an acidic pH. These soils are rooted in silicatic-siltic parent material, characterized by commendable drainage capabilities. Slopes within the basin exhibit two prominent soil types—Leptsols in steeper terrains and Cambisols in regions with more gentle gradients (Penna et al., 2017; Zuecco et al., 2018). These geological and soil attributes contribute significantly to the overall hydrological behaviour and environmental characteristics of the La Vizza basin offering crucial insights into the terrain's makeup and its hydrological implications.

2.2.Data and their sources

Basin topography is described by means of a DTM with a 25 m grid resolution (Fig.2). Precipitation, temperature data, streamflow/discharge at hourly time intervals and annual maxima of rainfall at 5 minutes intervals for the study basin are available from ARPAV (Agenzia Regionale per la Prevenzione e Protezione Ambentale del Veneto) for the period of 33 years (1 October 1985 to 31 September 2018). The observed discharge is available at the stream-gauge station in Cordevole Catchment at La Vizza for the study period. Precipitation and temperature data are obtained from the 11 different weather stations (Table 1) in and around the study area. The weather station, Passo Pordoi lies in the study basin which records both precipitation and temperature data (Fig.3).

Table 1: Details of weather stations. Data columns represent the type of data viz precipitation (P) and temperature (T) collected by corresponding station. Coordinates are in Monte Mario Rome Italy (1) projection system.

S.N.	Weather Station	X-Coordinate	Y-Coordinate	Data
1.	Arabba	1720708	5153542	P, T
2.	Caprile	1729697	5147256	P
3.	Biois a Cencenighe	1728252	5137397	P
4.	Falcade	1720777	5137469	P
5.	Malga Ciapela	1723204	5145688	P
6.	Passo Falzarego	1730654	5156004	P
7.	Passo Pordoi	1716656	5151560	P, T
8.	Passo Valles	1715621	5135470	P
9.	Pescul	1735771	5147134	P
10.	Selva di Cadore	1733595	5148836	P
11.	Pian Fedaia	1719830	5149000	P, T

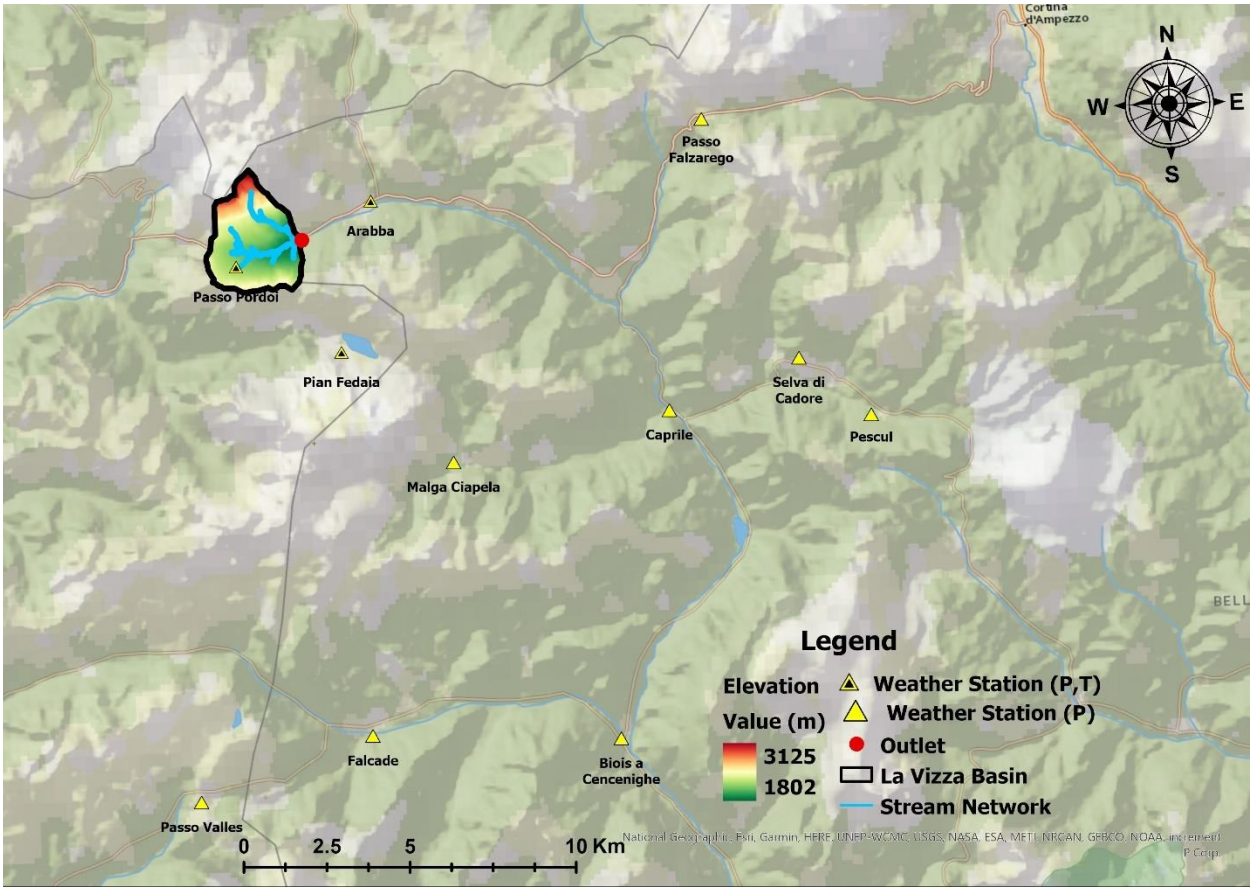

Fig 3: Location of the weather station. The yellow triangle indicates the weather station responsible for collecting precipitation data whereas and yellow triangle with black triangle inside indicates the weather station responsible for collecting both precipitation and temperature data.

Satellite observations-based MODIS snow cover area (SCA) data are available from the Institute for Applied Remote Sensing, EURAC research centre in coordination with the Bolzano province. It encompasses a comprehensive time span from 1 January 2003 to 31 December 2018. The data was meticulously curated at a spatial resolution of 250 meters. Notably, this endeavour hinged on the application of an algorithm grounded in MODIS observations, an approach pioneered by Notarnicola et al. (2013a, 2013b). The algorithm's efficacy lies in its capacity to generate MODIS maps that convey the categorical presence of snow, clouds, non-snow conditions (bare land), or water bodies, attributing these attributes to individual or clusters of pixels. Out of a collective of 374 corresponding pre-event instances, we have culled 326 pre-event MODIS images. These selected images boast a commendably low cloud cover percentage, clocking in at under 10%. This judicious selection paves the way for our rigorous analysis of the initial state of snow cover area (SCA) preceding each event.

3. Methods

3.1.Methodology for rainfall-runoff (rr) events selection

The purpose of rainfall-runoff events selection is to understand how the catchment responds to rainfall inputs. Rainfall-runoff event classifications serve as valuable tools for enhancing our comprehension of catchment hydrological dynamics (Gelmini et al., 2022). In the context of this study, the analysis encompasses rainfall-runoff events occurring October 1985 and September 2018. The selection of these events is predicated upon the application of specific criteria, aligning with standards used by Guastini et al. (2019). The listed criteria entail the following conditions:

a) a total event precipitation equal or larger than 5 mm,

b) two events were separated by at least 6 h with no precipitation (Guastini et al., 2019; Penna et al., 2011),

c) events with a difference between streamflow peak (Q_{peak}) and streamflow (Q) at the beginning of the event below 0.01mm/h are excluded. This was done by using constant-k method proposed by Blume et al. (2007).

For the chosen rainfall-runoff events, a comprehensive set of attributes was calculated. These attributes encompassed the duration of the rainfall, the cumulative precipitation, the average and maximum precipitation intensity, prevailing antecedent soil moisture and the streamflow peak (Table 2).

Table 2: Matrices used in the study for describing the rainfall-runoff events.

S.N.	Metrics
1.	Cumulative precipitation (mm)
2.	Precipitation duration (h)
3.	Average precipitation intensity (mm/h)
4.	Maximum precipitation intensity (mm/h)
5.	Runoff peak (m^3/s)
6.	Antecedent soil moisture

3.2. The hydrological model

3.2.1. TOPMELT and its integration into ICHYMOD

TOPMELT is an enhanced temperature-index based distributed continuous hydrological model for snowpack simulation that helps us understand how snow and glaciers melt (Zaramella et al., 2019). In other word, TOPMELT is a model that simulates how snow and ice melt in a mountain basin using temperature and solar radiation as inputs. To do this, it divides the basin into smaller areas based on their elevation and how much sunlight they receive. Higher areas are colder and lower areas are warmer, so elevation affects how fast snow and ice melt. Sunlight also affects melting, because more sunlight means more heat. TOPMELT uses a number of classes to group areas with similar sunlight levels. TOPMELT can calculate how much snow and ice melt in each class for each elevation band. Some areas may have glaciers, which are large masses of ice that move slowly. TOPMELT keeps track of how much glacier area there is in each class and elevation band, because glaciers melt differently than snow. The smaller the areas are, the more accurate the model is, but also the more time and resources it takes to run it. TOPMELT tries to balance accuracy and efficiency by choosing the right number of classes and elevation bands.

TOPMELT is based on the ICHYMOD hydrological model (Norbiato et al., 2008), which is a semi-distributed model that divides the basin into sub-basins and uses a lumped approach for each sub-basin. The ICHYMOD hydrological model is a tool that helps us understand how water flows through a river basin. It integrates TOPMELT model to simulate the movement of water from snowmelt and rainfall through the soil and into the river. The model has three parts: a snow routine, a soil moisture routine, and a flow routine which has been used for the purpose of this work.

The snow routine simulates how snow melts and turns into water. The snow routine in ICHYMOD represents snow accumulation and melt using a distribution function approach based on a combined radiation index degree-day concept (Norbiato et al., 2008). The degree-day method is a simple way to estimate the amount of snowmelt based on the air temperature. It assumes that the snowmelt is proportional to the difference between the air temperature and a base temperature, which is usually zero degrees Celsius. The proportionality constant is called the degree-day factor and it depends on the characteristics of the snow and the environment. The snow melt rate (M) is computed using the following equation:

$$M = \{ \begin{matrix} f_m EI(T_h - T_0), & T_h > T_0 \\ 0 & T_h > T_0 \end{matrix} \} \quad (1)$$

Where M is the melt rate (mm/h), T_h is the hourly mean temperature (°C), T_0 is a threshold temperature beyond which melt is assumed to occur (°C), f_m is a melt factor and EI is an energy index which represents the potential radiation energy (variable in time) for a given site in the basin (J/m^2h). This energy index is based on factors like the angle of the sun, how clear the sky is, the elevation of the area, which way it faces, and how steep it is.

The soil moisture routine describes how water is stored in the soil and how it moves through the ground. The soil moisture is calculated based on the probability distributed model (PDM) of the storage capacity, c, as described by Moore (2007) as following:

$$F(c) = 1 - (1 + \frac{c}{C_{max}})^b \quad (2)$$

Where C_{max} is the maximum soil water storage capacity per unit area, and parameter b is a Pareto exponent which controls the degree of spatial variability of storage capacity over the basin. The value of b is related to the spatial distribution of soil types and land use within the basin.

The flow routine calculates how water flows through the river basin. The model also considers how much water is lost due to evaporation and plant transpiration. The ICHYMOD model's streamflow routine, is designed to calculate the flow of water throughout the entire catchment area. It does this by considering two essential factors: the geographical layout of the land (topography) and the soil's hydraulic properties. This integrated approach provides a comprehensive understanding of the movement of water within the basin, taking into account both natural features and the characteristics of the soil.

3.2.2. Model validation

The model validation process involved a rigorous comparison between the simulated data generated by the model and the actual data observed in real-world scenarios. In this study, our focus was directed towards two critical types of data: outflow and snow cover area. The simulated

outflow values were meticulously cross-referenced with the measured discharge data collected at the La Vizza outlet throughout the study's duration. Similarly, we evaluated the congruence between the simulated snow cover area produced by the model and the satellite-derived snow cover data captured by MODIS observations. This comprehensive validation process was undertaken to ensure that the model's predictions were consistent and reliable in representing the real-world hydrological dynamics.

A normalized statistic, Nash-Sutcliffe efficiency (NSE) proposed by Nash & Sutcliffe (1970) is used in this work for comparing simulated and observed parameter. It assesses how closely a model's predictions align with real-world data. NSE serves as a valuable tool for evaluating the model's predictive accuracy by comparing its projections to actual outcomes. It quantifies the degree of fit between the model's projected values and the actual observations, represented by a line on a graph.

Bias is also calculated which is crucial in assessing the efficiency of a hydrological model as it provides insights into the systematic errors or deviations in the model's predictions. Bias refers to the consistent overestimation or underestimation of the model's output compared to the observed data.

In this work, Nash-Sutcliffe efficiency (NSE) and bias are calculated for outflow and snow cover area by using the following statistics:

$$\mathrm{NSE} = 1 - \frac{\sum_{i=1}^{N} (\mathrm{OBS_i} - \mathrm{SIM_i})^2}{\sum_{i=1}^{N} (\mathrm{OBS_i} - \overline{\mathrm{OBS}})^2} \tag{3}$$

$$\mathrm{Bias} = \frac{\sum_{i=1}^{N} (\mathrm{SIM_i} - \mathrm{OBS_i})}{\sum_{i=1}^{N} \mathrm{OBS_i}} \tag{4}$$

where OBS_i and SIM_i are the observed and simulated parameter at time i, respectively, $\overline{OBS}$ is the average value of the observed parameter and N is the number of observations.

The ideal values for bias and Nash–Sutcliffe efficiency (NSE) are 0 and 1, respectively. An NSE value of 1 signifies a perfect match between the model's predictions and the observed data, while an NSE value of 0 indicates that the model's predictions are equivalent to the average of the

observed data. NSE values falling between negative infinity and 0 suggest that the observed data's average provides better predictions than the model.

3.3.Trend analysis

Trend analysis in hydrometeorology serves as a valuable tool for unravelling the intricate interactions between climatic shifts and hydrological processes within a mountain basin (Kliment et al., 2011) is crucial for comprehending the hydrological dynamics of a basin due to its capacity to unveil long-term shifts and patterns in climatic and hydrological variables. By examining trends, we can identify significant changes in hydrometeorological variables. In this study trend analysis are done for the variable such as annual maxima of rainfall, annual maxima of runoff, mean annual temperature, antecedent soil moisture conditions and antecedent snow water equivalent at annual and seasonal time scale. This analysis helps us understand the evolving behaviour of these variables, their potential impacts on the basin's water resources and reasons for the divergence trends in rainfall-runoff events.

In the field of hydro climatology, methods for identifying significant trends in time series data can be categorized into two main types: parametric and non-parametric approaches (Gocic & Trajkovic, 2013). Parametric tests demand that the data is both independent and follows a normal distribution, while non-parametric tests only necessitate data independence. In the context of this study, two non-parametric methods, namely the Mann-Kendall test and Sen's slope estimator, are employed to identify trends in hydrometeorological variables. These methods offer robust trend detection capabilities and are particularly suitable for analysing the intricate dynamics of the dataset.

3.3.1. Man-Kendall test

The Mann-Kendall test, also known as the Kendall's tau test, is a non-parametric statistical test widely used to detect trends within hydrometeorological variables with time series data (Birsan et al., 2005; Brabets & Walvoord, 2009; Diop et al., 2018; Kliment et al., 2011; Soltani et al., 2013; Umar et al., 2022; Wu & Qian, 2017) has been used in this study. It assesses whether there is a monotonic increasing or decreasing trend in the data over time. The test statistic S for the Mann-Kendall test (Kendall, 1975; Mann, 1945) is calculated using the following formula:

$$S = \sum_{i=1}^{n-1} \sum_{j=i+1}^{n} \mathrm{sgn}(x_j - x_i) \quad (5)$$

Where, n is number of observations, x_j and x_i are the rank of the k^{th} and i^{th} observation respectively where j>i and sgn(x_j- x_i) is sign function given by:

$$sgn(x_j - x_i) = \begin{cases} +1, & if\ x_j - x_i > 0 \\ 0, & if\ x_j - x_i = 0 \\ -1, & if\ x_j - x_i < 0 \end{cases} \quad (6)$$

The variance is calculated using the following formula:

$$Var(S) = \frac{(n-1)(2n+5) - \sum_{i=1}^{m} t_i(t_i-1)(2t_i+5)}{18} \quad (7)$$

Where, the symbol "n" signifies the total number of data points, "m" represents the count of tied groups within the dataset, with each tied group consisting of data points that share the same value. The variable "t_i" signifies the number of ties within each tied group of a particular extent "i". For sample size greater than 10 (n>10), the calculation of the standard normal test statistic denoted as "Z_S" is performed using Equation (8).

$$Z_s = \begin{cases} \frac{S-1}{\sqrt{Var(S)}}, & \text{if } S > 0 \\ 0, & \text{if } S = 0 \\ \frac{S+1}{\sqrt{Var(S)}}, & \text{if } S < 0 \end{cases} \quad (8)$$

The underlying principle of the Mann-Kendall test involves testing the null hypothesis (H_0), which asserts the absence of a significant trend within the dataset. The rejection of the null hypothesis implies the presence of a considerable trend within the data series. The process of testing these trends is conducted at a specified significance level denoted as "α." When the calculated value of Z_S exceeds a critical value, the null hypothesis is rejected. This indicates the existence of a statistically significant trend within the time series under examination. The critical value is derived

from the standard normal distribution table. In this study, level of significance (α) of 5% is considered for the Man Kendall statistics test. At a significance level of 5%, the null hypothesis of no trend is rejected if the absolute value of $|Z_S|$ exceeds 1.96.

Positive values of the standard normal test statistic, Z_S, hold significance in the context of trend analysis. These positive values point towards increasing trends within the examined time series data. Conversely, when Z_S assumes negative values, this suggests the presence of decreasing trends in the data.

3.3.2. Sen slope estimator

The Mann-Kendall test serves the purpose of determining whether a significant trend exists within a dataset. It answers the question of whether any noteworthy trend, whether upward or downward, can be identified. However, the test itself does not provide information about the magnitude of the detected trend.

To address this aspect, another technique known as Sen's slope estimator, a non-parametric procedure is applied. This method, developed by Sen (1968), is employed to calculate the actual magnitude of the trend observed in the dataset. For a given dataset containing N sample pairs, the slope representing the magnitude of the trend is computed using a following formula:

$$Q_i = \frac{X_j - X_k}{j-k} \text{ for } i = 1, \ldots, N \quad (9)$$

In equation 9, the terms x_j and x_k correspond to the data values associated with distinct time indices denoted as 'j' and 'k', respectively. 'j' refers to a particular time, while 'k' represents an earlier time point.

In case where there is only a single data value for each time period, the total number of paired samples, $N = \frac{n(n-1)}{2}$; n is the number of time periods. For multiple observation in one or more time periods, $N < \frac{n(n-1)}{2}$ is used.

After obtaining the 'N' values of Q_i, they are organized in ascending order from the smallest to the largest. Subsequently, the median of the slopes, often referred to as Sen's slope estimator, is computed from these ordered values by using following formula:

$$Q_{med} = \begin{cases} Q_{\left[\frac{N+1}{2}\right]}, & \text{if N is odd} \\ \frac{Q_{\left[\frac{N}{2}\right]} + Q_{\left[\frac{N+2}{2}\right]}}{2}, & \text{if N is even} \end{cases} \quad (10)$$

The sign of Q_{med} represent the trend exhibited by the data, while its magnitude signifies the degree of the trend's steepness.

3.4. Remote sensing tools for snow cover area calculation and MODIS image selection for validation

Based on remote sensing tools, satellite observations-based MODIS snow cover area (SCA) data are available from the Institute for Applied Remote Sensing, EURAC research centre. These records are generated by amalgamating snow maps derived from both MODIS Terra and Aqua sensors (Gafurov & Bárdossy, 2009; Mölg et al., n.d.; Wang & Xie, 2009). It is important to note that these sensors operate with different acquisition modes and times, with Terra acquiring data in the morning in descending mode and Aqua collecting information in late morning or afternoon in ascending mode. This variation in acquisition times results in reduced cloud coverage and fewer pixels devoid of valuable data, owing to distinct lighting conditions and satellite viewing angles. In the context of this study, the EURAC centre provides MODIS snow cover area (SCA) data, which is based on the algorithm developed by Notarnicola et al. (2013a, 2013b). This algorithm offers categorical SCA data at a spatial resolution of 250 meters, as delineated in Table 3.

Table 3: EURAC MODIS product description.

S.N.	MODIS product	EURAC code
1.	Not detected	0
2.	Snow	1
3.	No Snow/bare land	2
4.	Cloud	3
5.	Surface water body	5

3.4.1. Fractional snow cover area calculation

To verify the accuracy of the model's simulated fractional snow cover area derived from the TOPMELT algorithm, a comparison was made with the satellite observations-based MODIS snow cover area (SCA). In line with the methodology employed by Di Marco et al. (2020), the MODIS

snow cover area was also converted into fractional snow cover area. This conversion process involves calculating the ratio between the number of pixels identified as snow-covered and the total count of pixels, excluding those obscured by clouds. This relationship is expressed through Equation 11.

$$\text{fSCA} = \frac{N_{Snow}}{N_{tot} - N_{clouds}} \tag{11}$$

where, N_{snow} represents the count of pixels indicating snow cover in the MODIS dataset, N_{tot} signifies the total number of pixels encompassing the entire catchment area, and N_{clouds} accounts for the pixels identified as clouds by the MODIS classification.

3.5. Method for selection of MODIS SCA for validation with model simulated SCA

To enhance the accuracy for validating the simulated snow cover area (SCA) with real ground data, specific criteria are employed to refine the satellite-based MODIS images. These criteria are designed to closely approximate the actual snow cover area on the ground. The following conditions are applied to refine the MODIS images:

i. Select MODIS image before the rainfall-runoff event with cumulative precipitation less than 10 mm of rainfall. This selection criteria based on the understanding that intense rainfall exceeding 10 mm has the potential to induce snowmelt, thereby distorting the accurate representation of the actual snow cover conditions preceding the rainfall-runoff event.

ii. Select MODIS image with least possible cloud coverage before the rainfall-runoff event. This approach is adopted to reduce the potential overestimation of Snow-Covered Area (SCA) that could result from the inclusion of cloud-covered regions in the calculation. In pursuit of this, MODIS images taken up to one week prior to the rainfall event are examined thoroughly.

4. Results

4.1.Rainfall-runoff events

To examine how the catchment responds to rainfall and the role of soil moisture in the runoff process, a total of 944 rainfall-runoff events were selected between 1985 and 2018 using the criteria described in section 3.1 of the methodology. Out of these 944 rainfall-runoff events, 512 occurred between the years 2003 and 2018, during which MODIS images of snow cover area were available for comparison and validation of the results.

4.2.Model validation

The model's accuracy was assessed through a comparison of its simulated results with real-world observations. This evaluation was conducted by employing the Nash-Sutcliffe efficiency (NSE) and bias calculations, as outlined in section 3.2.2 of the methodology. In this study, two key parameters, namely runoff and snow cover area, were utilized to gauge the model's effectiveness.

For the entire study period, the NSE and bias values for the runoff were computed and yielded values of 0.48 and -0.0041, respectively. An NSE score of 0.48 indicates a moderate level of agreement between the model's predictions and the actual observed runoff data. Similarly, a bias value of -0.0041 suggests that the model's predictions do not exhibit significant overestimation or underestimation tendencies when compared to the observed data.

For the snow cover area assessment, the NSE was calculated specifically for the period spanning from 2003 to 2018, while excluding summer events. The value for NSE was found to be 0.31 signifying a moderate agreement between the model's predictions and the actual observed snow cover area data. The reduction in the Nash-Sutcliffe Efficiency (NSE) value could potentially be attributed to the disparity in temporal resolution concerning the snow cover data. In the context of the MODIS observation, a solitary instance of snow cover area data is acquired within a day, as opposed to the model-generated dataset which encompasses 24 distinct snow cover data points. This incongruence in temporal data granularity may plausibly account for the observed decrement in the NSE, specifically in relation to the representation of snow cover area.

4.3. Trend analysis

The assessment of trends was conducted on various variables, including the annual maxima of rainfall, the annual maxima of runoff, mean annual temperature, antecedent snow water equivalent, and antecedent soil moisture. This analysis encompassed both annual and seasonal timeframes and was carried out using the non-parametric Man-Kendall test at , a significance level (α) of 0.05 and Sen slope estimator, following the methodology described in section 3.3.

4.3.1. Trends in annual maxima of rainfall

The application of Mann-Kendall and Sen's slope statistical tests reveals a mix of positive, negative, and no trends in the annual maxima of rainfall. Notably, a prevailing increasing trend has been detected in the annual maxima for a significant portion of rainfall durations (Annex 1).

In Fig 4, only trends in the annual maxima of rainfall for three weather stations is shown for the annual maxima of rainfall at 15 minute, 30 minute, 45 minute, 1 hour, 3 hour, 6 hour, 12 hour and 24 hours duration.

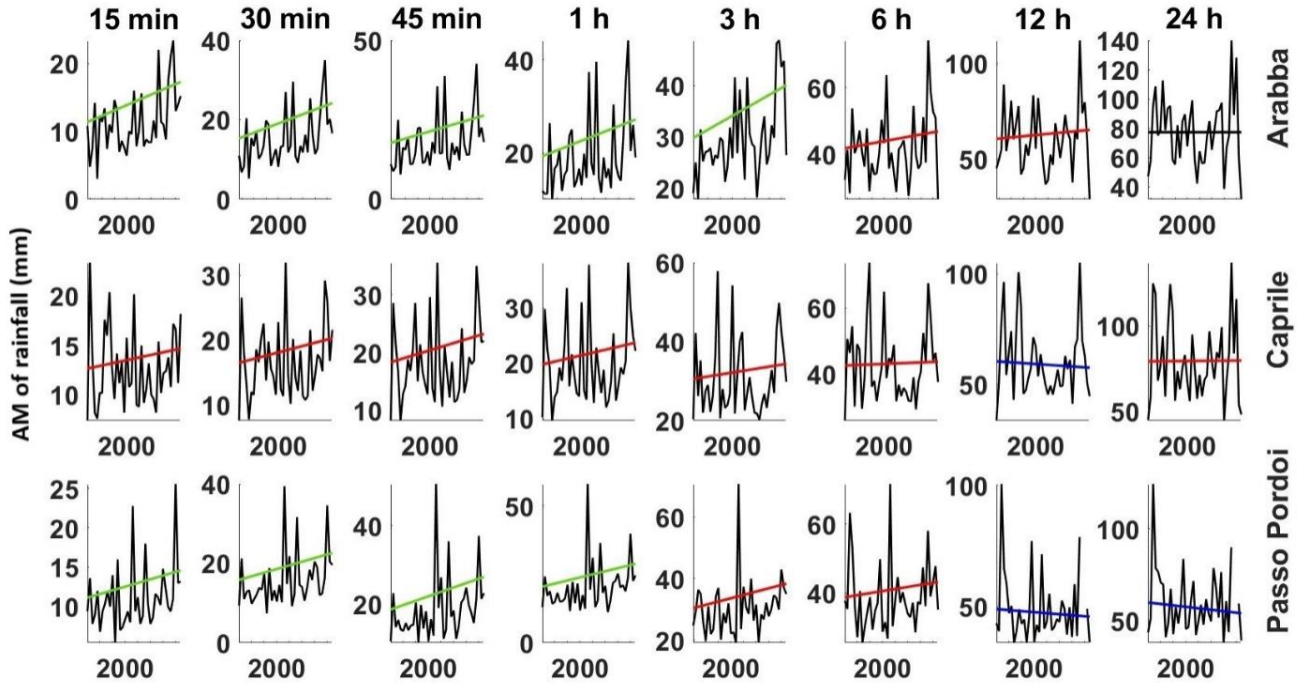

Fig 4: Trends in the annual maxima of rainfall. Red, blue, green line indicate the presence of trends while black line indicates no trend in annual maxima. Among these, both the red and green trend

lines signify increasing trends, with the green trend line being statistically significant (at α=5%). On the other hand, the blue line depicts statistically insignificant decreasing trends.

Out of the total trends identified in the annual maxima of rainfall for various durations, approximately 76% exhibit positive trends (Fig. 5), indicating an increase over time. Conversely, about 23% demonstrate negative trends, signifying a decrease, while around 1% exhibit no trend. Notably, among all the detected trends, only 25% are statistically significant, and interestingly, all of these significant trends are positive, indicating a noteworthy and consistent increasing trend in the annual maxima of rainfall.

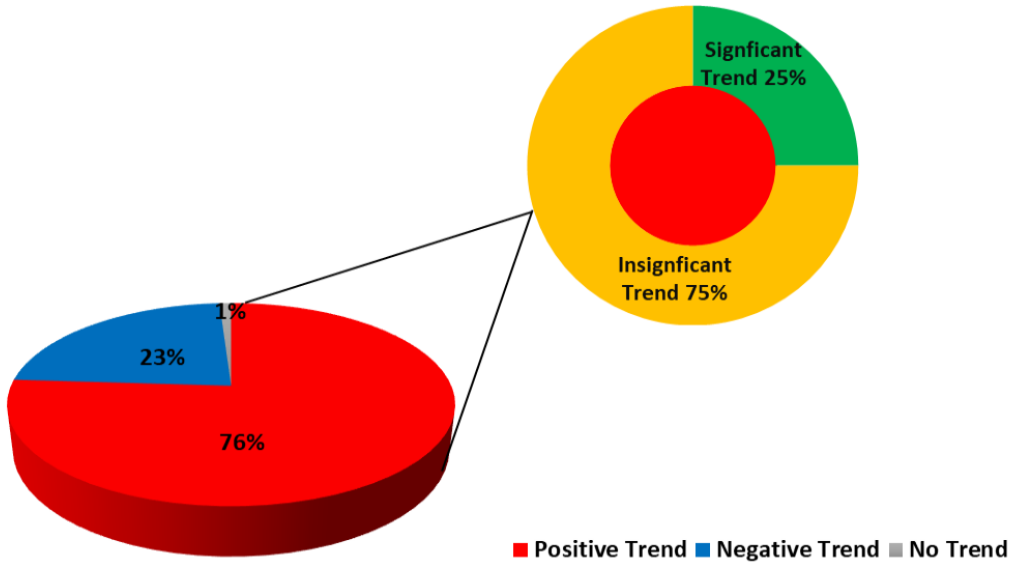

Fig 5: Percentage of trends in the annual maxima of rainfall for various duration of rainfall. Red, blue, and grey colour section indicates respectively the presence of positive, negative and no trends in annual maxima of rainfall.

The analysis has identified statistically significant increasing trends in the annual maxima of rainfall for various durations, specifically at intervals of 5 minutes, 10 minutes, 15 minutes, 30 minutes, 45 minutes, 1 hour, and 3 hours, consistently observed across multiple weather stations. Notably, the most prominent increase, reaching up to 12.30%, is seen in the annual maxima of rainfall for a 30-minute rainfall duration over a span of 10 years (Fig. 6). This significant finding underscores a clear pattern of rising annual maxima for shorter rainfall durations, which becomes evident when considering the data presented in Annex 2.

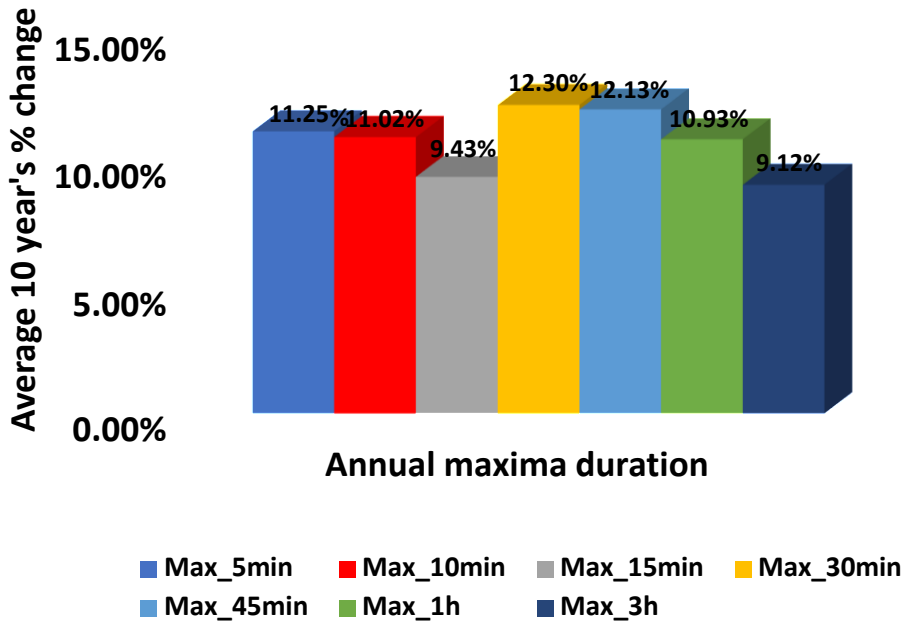

Fig 6: Average percentage change in significant annual maxima duration in a decade time.

4.3.2. Trends in annual maxima of runoff

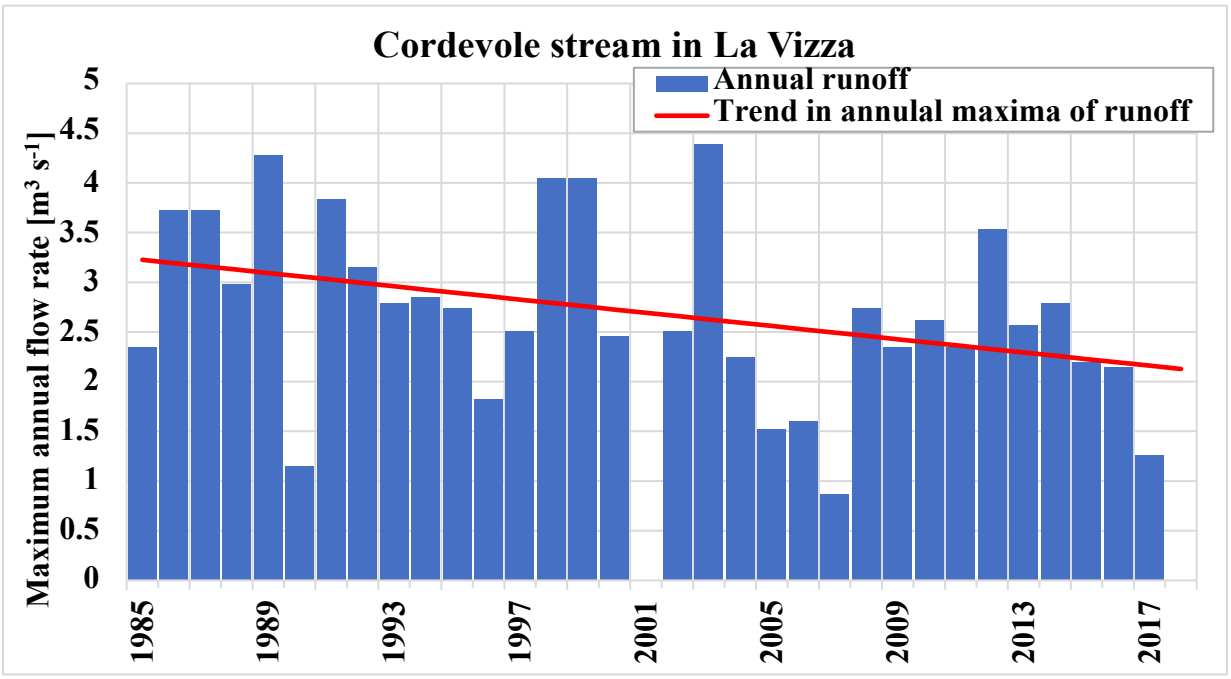

Fig 7: Trend in the annual maxima of runoff

The analysis has identified statistically significant decreasing trends in the annual maxima of runoff peak (Fig. 7). This analysis revealed a decrease of -10.7% in the annual maxima of runoff in a decade.

4.3.3. Trends in mean annual temperature

Upon subjecting the data to Mann-Kendall and Sen's slope statistical tests, a robust pattern of statistically significant increasing trends in the mean annual temperature is found across all the weather stations (Annex 2). This noteworthy observation is vividly represented in Fig.7, illustrating a consistent increase in the mean annual temperature within the study basin. This finding provides a clear and compelling elucidation of the progressively rising mean annual temperature in the vicinity of the study area.

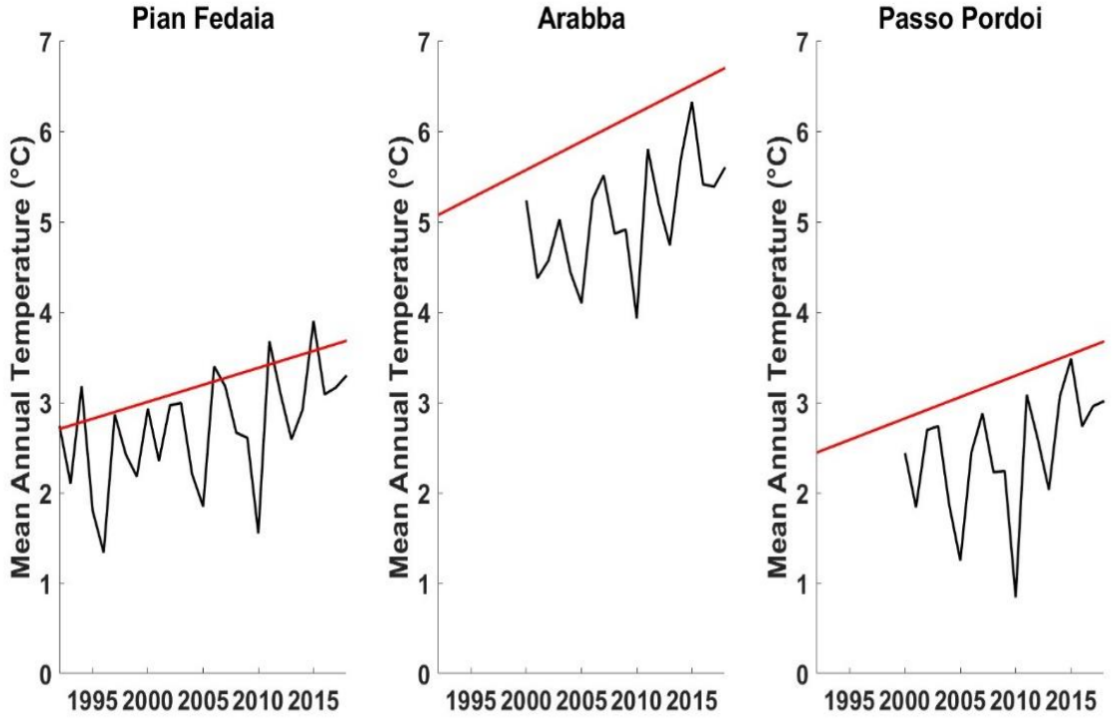

Fig 8: Scatter plot with trends in the mean annual temperature. Red trend line indicates statistically significant positive trend.

Across the given weather stations, there is a notable range in the increase of mean annual temperature, ranging from 12.34% to 19.37% over a span of 10 years (Fig. 8). To derive a comprehensive perspective, the average mean annual temperature increase has been calculated by computing the mean of observed temperature increments. This calculation yields a significant

value of 15.19% rise over a decade, equivalent to a rise of 0.49 ° Celsius. This analysis effectively captures the overall trend of temperature escalation within the designated timeframe.

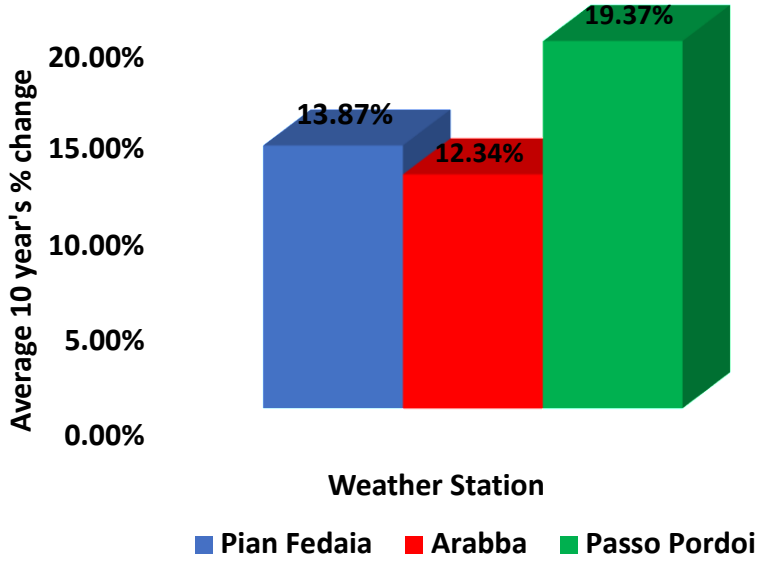

Fig 9: Percentage change in the mean annual temperature for 10 years' time

4.3.4. Trends in antecedents SWE at annual and seasonal timescale

A negligible negative trend has been found for the antecedent Snow Water Equivalent (SWE) at the annual timescale (Fig 10). However, when shifting the focus to the seasonal timescale, a distinct pattern emerges. Notably, a marked positive trend, characterized by a significant magnitude, becomes apparent for the winter season. In contrast, significant negative trends is observed for the spring season, while smaller negative trends are detected for the autumn period. Intriguingly, no discernible trend is identified for the summer season, as shown in Fig 11. It is crucial to highlight that, upon closer inspection of statistical significance (as detailed in Annex 3), the previously noted positive trend for the winter season is deemed insignificant. When this factor is taken into consideration, the analysis conclusively indicates the presence of decreasing trends in the Snow Water Equivalent.

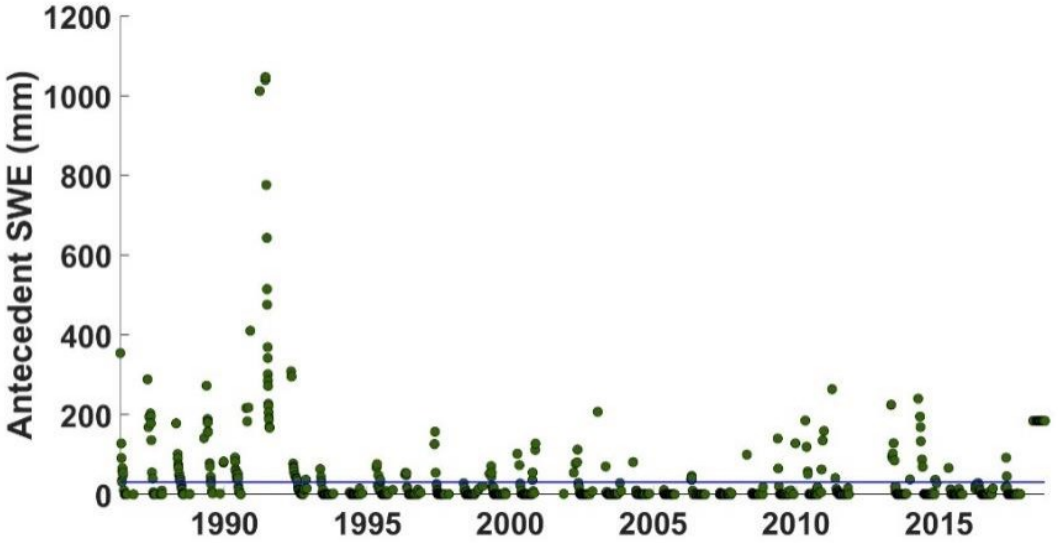

Fig 10:Scatter plot with trend in antecedents SWE at annual timescale

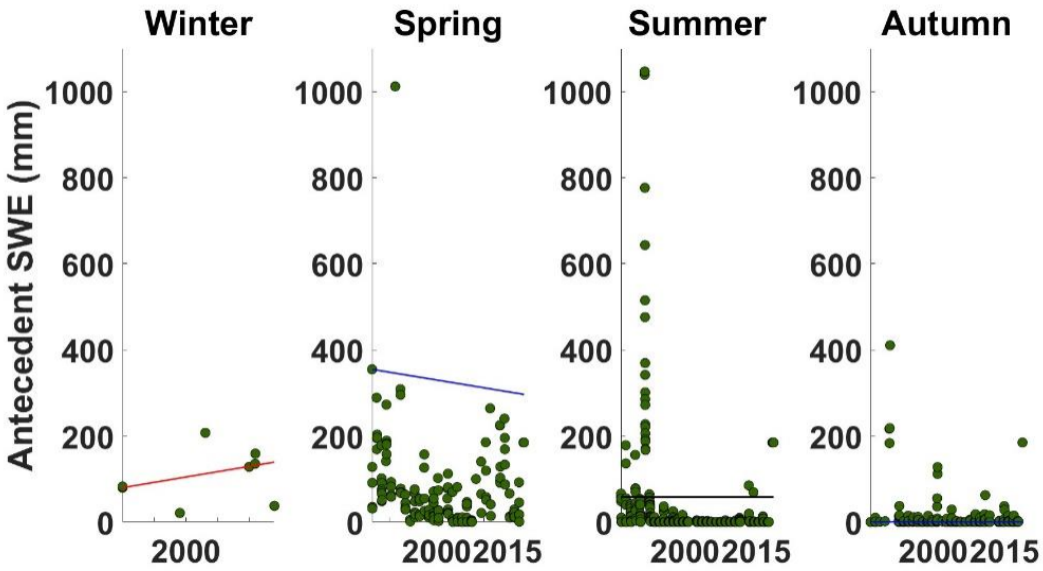

Fig 11: Scatter plot with trend in antecedents SWE at seasonal timescale. Red trend line indicates increasing trend and blue trend line indicates decreasing trend and black line indicates no trend.

When examining the antecedent snow water equivalent, a markedly positive trend during the winter season indicates substantial snowpack accumulation. This could be the result of increased snowfall or reduced melting rates but since there is limited data point in the winter, there could

also be no trend as well. Conversely, substantial negative trends during spring suggest rapid snowpack depletion, potentially due to warmer temperatures and accelerated snowmelt. Smaller negative trends in autumn indicate a gradual reduction in snow water equivalent leading up to winter. Notably, no discernible trend in summer implies that there is no significant accumulation or reduction in snow water equivalent during this season.

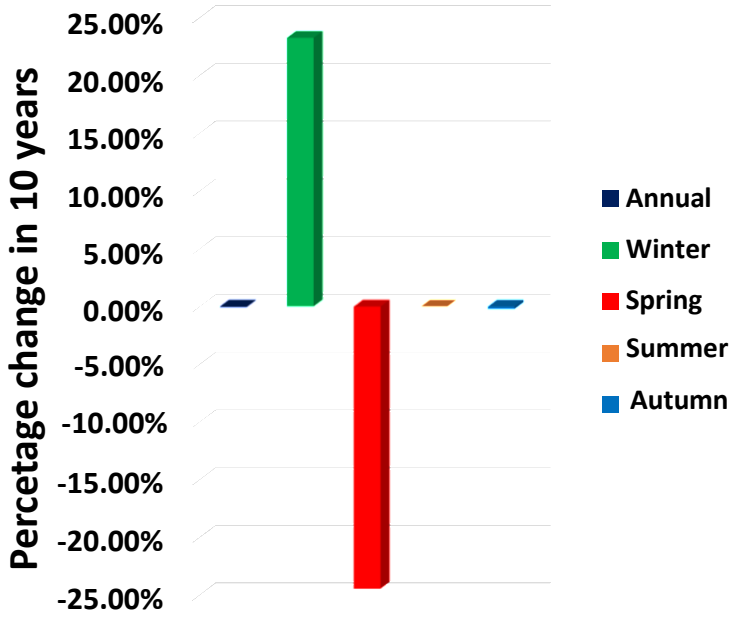

Fig 12: Percentage change in antecedents SWE in a decade

When considering statistics, a striking finding surfaces: a noteworthy and statistically significant decrease in the antecedent Snow Water Equivalent (SWE) is evident across both annual and seasonal timescales (Annex 4). The most prominent decline in the antecedent SWE by 24.46% has been found, specifically within the spring season, over a decade-long span (Fig. 12). This result underscores a significant alteration in the snow water equivalent, emphasizing the pronounced shift observed in the springtime SWE dynamics.

4.3.5. Trends in antecedent SM at annual and seasonal timescale

At the annual timescale, a negligible negative trend is discernible in the antecedent soil moisture (Fig. 13). Upon shifting the focus to the seasonal timescale, distinct observations emerge. Notably, positive trends are detected for the summer, winter, and autumn seasons, while conversely, a

negative trend is identified for the spring period, as visually depicted in Fig. 14. It is essential to emphasize that, upon closer scrutiny (Annex 4), all of these identified trends lack statistical significance at the 5% level of significance. This underscores that the observed variations in antecedent Soil Moisture, although noticeable, do not attain a level of statistical significance within the specified confidence interval.

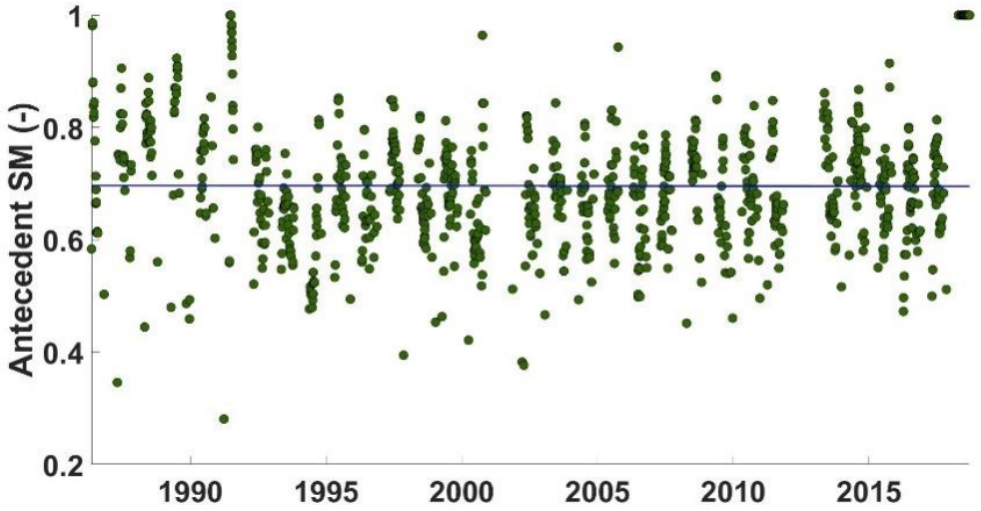

Fig 13:Scatter plot with trend in antecedents SM at annual timescale. Blue trend line indicates decreasing trend.

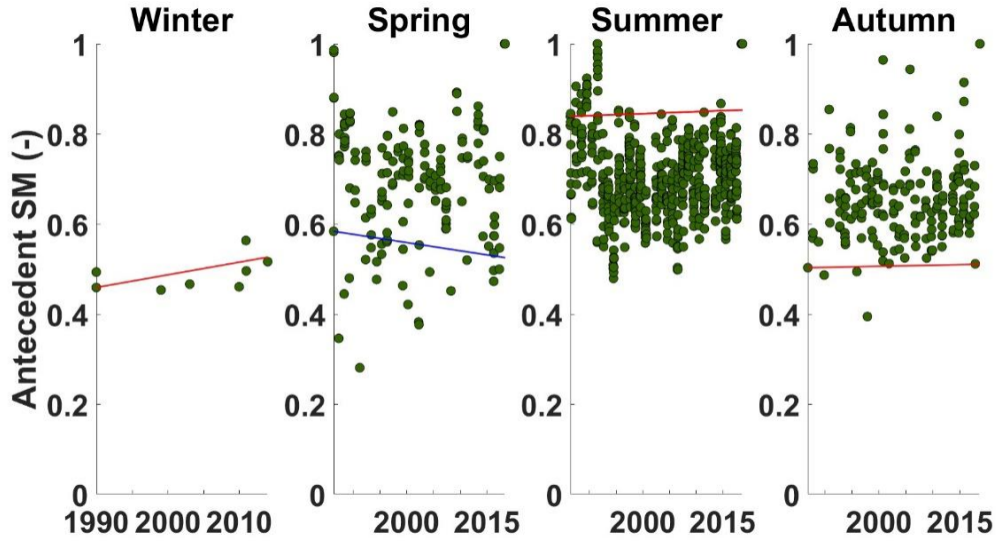

Fig 14: Scatter plot with trends in antecedents SM at seasonal timescale. Red trend line indicates increasing trend and blue trend line indicates decreasing trend.

During summer, winter, and autumn, positive trends in antecedent soil moisture suggest that the soil tends to retain more moisture over time, potentially due to factors like increased rainfall or reduced evaporation. However, the limited numerousness in winter hinders the understanding of soil moisture trends. Conversely, the negative trend in antecedent soil moisture during spring implies a drying trend leading up to this season, possibly attributed to factors such as increased evaporation or decreased precipitation in preceding months.

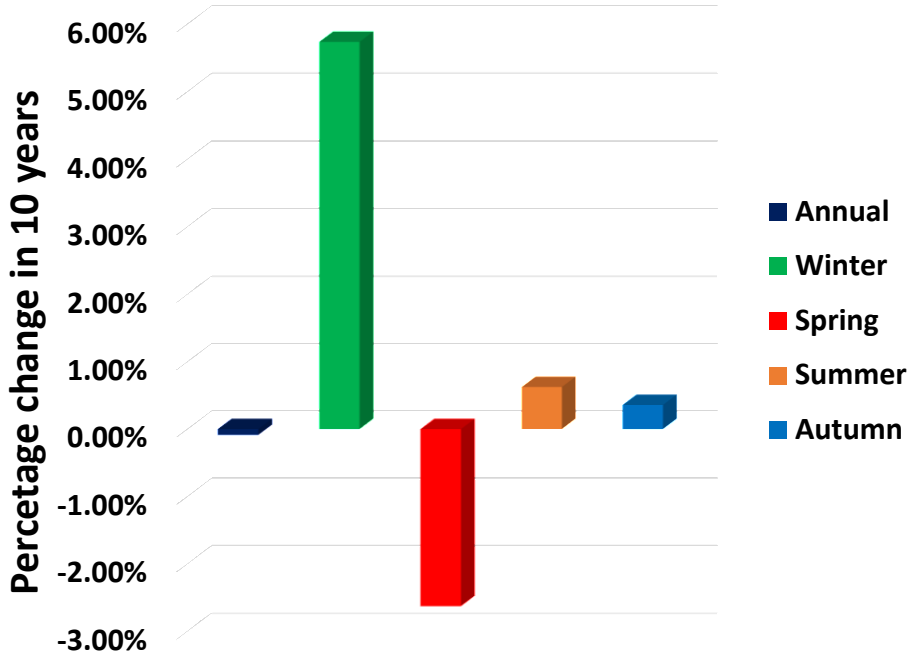

Fig 15: Percentage change in antecedents SM in 10 years' time

Over a span of 10 years, an intriguing pattern has emerged within the antecedent Soil Moisture (SM) dynamics, as illustrated in Fig. 15. The maximum increase, reaching 5.74%, is in the antecedent SM in winter, while the maximum decrease of 2.63% is in the spring season. Although none of these trends exhibit statistical significance, it's worth noting that the spring trend comes closest to being statistically significant, with a p-value of 0.08. This finding highlights the notable fluctuations in soil moisture content within the specified timeframe, underscoring the dynamic nature of the studied parameter.

4.3.6. Trends in event characteristics

The study examined trends in event attributes like cumulative precipitation, average precipitation intensity, streamflow peak, and runoff coefficient. The analysis employed statistical methods including Man-Kendall statistics and the Sen slope estimator. The objective was to gain insights into how these event characteristics contribute to shaping the trends observed in runoff events.

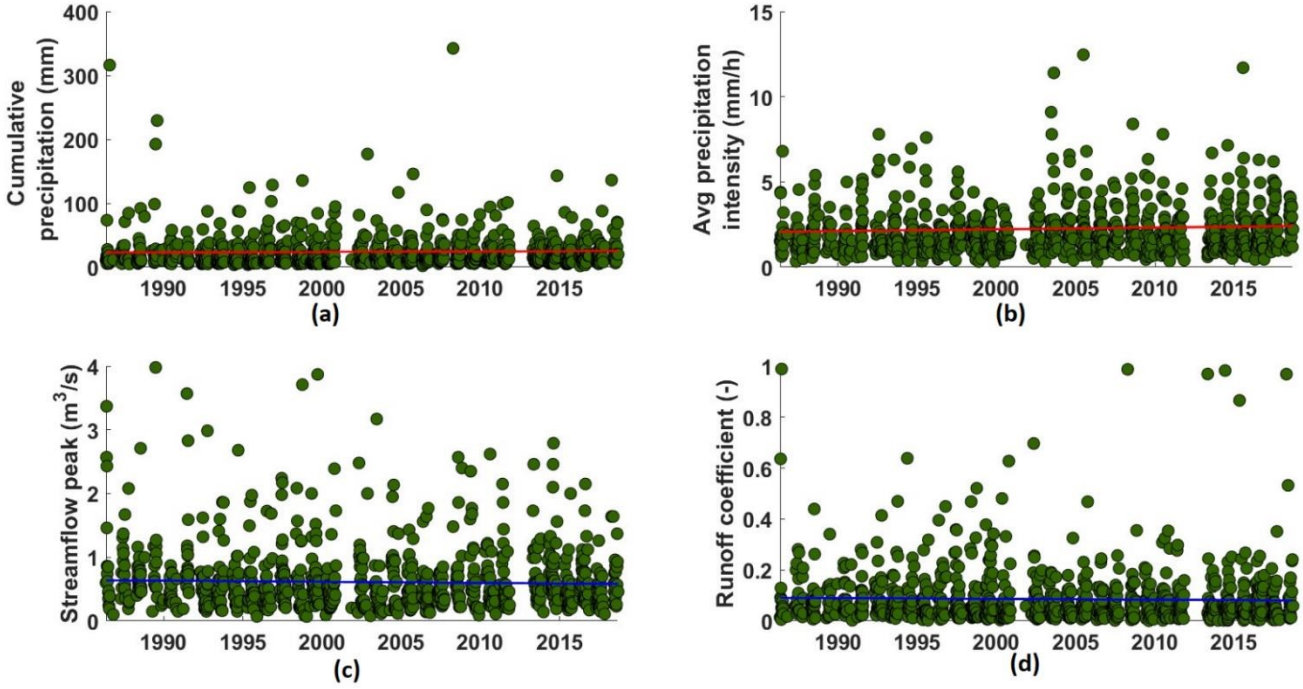

Fig 16: Scatter plot with trend in event characteristics in (a) cumulative precipitation, (b) average precipitation intensity, (c) streamflow peak, (d) runoff coefficient. Red and blue trend line indicate positive and negative trend respectively.

The analysis conducted using the statistical methods of Man-Kendall test and Sen slope estimator for event characteristics yielded important insights. These findings indicated the presence of significant positive trends in cumulative precipitation and average precipitation intensity. Conversely, negative trends were observed in both streamflow peak and runoff coefficient, as illustrated in Fig. 16. However, it's essential to emphasize that the observed negative trend in streamflow peak did not attain statistical significance at the specified significance level (α) of 0.05 (Annex 5).

An examination of the data revealed a notable rise in cumulative precipitation by 3.62% and in average rainfall intensity by 4.81% over a span of ten years within the context of rainfall events.

On the contrary, for the same period, a decline of 2.8% in streamflow peak and 3.5% in runoff coefficient was observed (Fig 17).

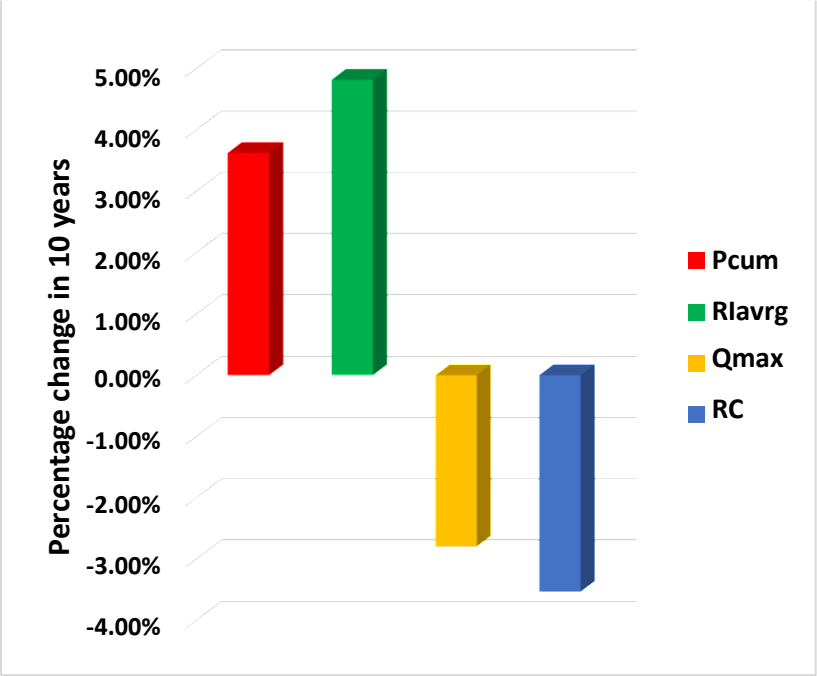

Fig 17: Percentage change in event characteristics in a decade

5. Discussion

5.1. Trend divergence in annual maxima of rainfall and annual maxima of runoff

A positive increasing trend in the annual maxima of rainfall, as reported in section 4.3.1 of the results, aligns with studies conducted by De Michele et al. (1998) and Montanari et al. (1996) for northern Italy. Similar findings were demonstrated in the study carried out by Madsen et al. (2014) for Europe. The findings from another study by Caloiero et al. (2011) also support the increasing trend in annual maxima of rainfall.

Negative decreasing trend results emerged in the context of annual maxima of runoff, as reported in section 4.3.2 of the results, aligned with the study conducted by Mason (2023) for the La Vizza basin. This result is also supported by the study of Madsen et al. (2014), which indicates a decreasing trend in annual maxima of runoff. This trend was also evident in other studies from regions dominated by snow in Europe.

The increasing trend in annual maximum rainfall suggests that the region is experiencing more intense rainfall events, as evident from section 4.3.6 of the results. This can lead to higher water input into the river systems. However, the decreasing trend in annual maxima of runoff implies that this increased rainfall is not translating into an equivalent increase in river discharge. This discrepancy could be due to various factors affecting hydrological processes, but in this study, we tried to understand the role of the antecedent SWE and soil moisture conditions on the runoff generation. The trend analysis of antecedent snow water equivalent and antecedent soil moisture conditions, both on an annual timescale from sections 4.3.4 and 4.3.5 of the results respectively, indicates that snow water equivalent is significantly decreasing, while soil moisture is decreasing negligibly. The reduction in snow water equivalent (SWE) correlates with a decrease in the snowpack, resulting in a decreased volume of meltwater for runoff generation in snow-dependent regions. This process involves decreased snow accumulation during winter, with the subsequent warming in spring initiating the snowmelt, which contributes significantly to streamflow. Lower SWE translates to a reduced snowpack available for meltwater, thus diminishing the volume of meltwater entering watercourses and subsequently decreasing the runoff peak.

From the trend analysis of mean annual temperature from sections 4.3.3 of the result, it is evident that temperatures are consistently increasing. The calculation yields a significant value of a 15.19% rise over a decade, equivalent to a rise of 0.49°C in mean annual temperature. The increasing trend in mean annual temperature, as evident from this study, has implications for changing water dynamics in the basin due to melting snow cover. The melting of snow cover, primarily attributed to increasing temperatures, reveals a cascade of hydrological consequences. Snow meltwater, which plays a pivotal role in sustaining streamflow during warmer months, indicates shifts in timing and magnitude of runoff. Consequently, alterations in the availability of meltwater would have significant impacts on runoff patterns, accentuating the observed divergence between rainfall and runoff trends.

5.2. Trends in hydrometeorological variables and influence of antecedent's snow water equivalent and antecedent's soil moisture in runoff process

The implications of the observed trends in cumulative precipitation, average precipitation intensity, streamflow peak, and runoff coefficient, as determined by the Man-Kendall test and Sen slope estimator, are significant when considering the role of antecedent soil moisture (slightly decreasing) and antecedent snow water equivalent (significantly decreasing in spring) in runoff events.

The result obtained as in section 4.3.6 for rainfall intensity shows increasing trend in the rainfall intensity which is in the line with the study conducted by Brunetti et al. (2001) for the northern Italy. The increasing trend in the rainfall intensity was also demonstrated in the study conducted by Caloiero et al. (2011). The notable increase in cumulative precipitation (3.62%) and average rainfall intensity (4.81%) over a decade indicates a changing precipitation pattern.

The observed decline in streamflow peak (2.8%) and runoff coefficient (3.5%) over a decade justify a reduction in the magnitude of runoff generated from rainfall events as obtained in the section 4.3.2 of the result. This could be due to various factors, one of which is antecedent soil moisture. Since, the trend in the soil moisture content before a rainfall event is decreasing, the soil can absorb more of the incoming precipitation, reducing the immediate generation of surface runoff in the future. As such, changes in antecedent soil moisture can influence the runoff response to rainfall.

While there's a negligible decrease in antecedent SWE, it's important to note that changes in snowpack dynamics can significantly affect runoff, especially in regions where snowmelt is a significant contributor to streamflow like La Vizza basin. Changes in SWE can influence the timing and magnitude of snowmelt runoff. Even small changes can impact the overall hydrological regime, affecting the availability of water during different seasons.

6. Conclusion

The assessment of trends in rainfall-runoff events in the La Vizza mountain basin has yielded valuable insights into the changing hydrological dynamics of the region. Notably, there is a clear divergence between the trends in annual maxima of rainfall and annual maxima of runoff. While annual maxima of rainfall have exhibited a significant upward trajectory, annual maxima of runoff have experienced a marked decrease over the same period. This divergence between increasing rainfall and decreasing runoff suggests that the hydrological response to precipitation events is undergoing notable changes.

The analysis of hydrometeorological variables, including cumulative precipitation and average rainfall intensity, indicates a shifting precipitation pattern characterized by more intense rainfall events. These changes, combined with the decreasing trend in antecedent soil moisture, imply that initial soil conditions are becoming drier before rainfall events. This, in turn, can lead to increased infiltration capacity, reduced surface runoff. Moreover, the observed trends in antecedent snow water equivalent underscore the significance of snowpack dynamics in influencing runoff patterns, particularly in regions largely dependent on snowmelt for streamflow.

In light of these findings, several recommendations emerge. Firstly, there is a pressing need for further research to understand the multifaceted factors influencing these trends, including land use changes, evapotranspiration rates, and soil properties. The use of hydrological models like the ICHYMOD and TOPMELT has proven valuable in understanding the role of initial conditions of parameters like soil moisture and snow water equivalent in runoff events in absence of observed data. Further refinement and application of such models can enhance predictive capabilities and inform sustainable water resource management practices.

7. References

Arnbjerg-Nielsen, K. (2006). Significant climate change of extreme rainfall in Denmark. *Water Science and Technology*, *54*(6–7), 1–8.

Beniston, M., Farinotti, D., Stoffel, M., Andreassen, L. M., Coppola, E., Eckert, N., Fantini, A., Giacona, F., Hauck, C., & Huss, M. (2018). The European mountain cryosphere: a review of its current state, trends, and future challenges. *The Cryosphere*, *12*(2), 759–794.

Birsan, M.-V., Molnar, P., Burlando, P., & Pfaundler, M. (2005). Streamflow trends in Switzerland. *Journal of Hydrology*, *314*(1–4), 312–329.

Blume, T., Zehe, E., & Bronstert, A. (2007). Rainfall—runoff response, event-based runoff coefficients and hydrograph separation. *Hydrological Sciences Journal*, *52*(5), 843–862.

Bocchiola, D., Catalano, F., Menduni, G., & Passoni, G. (2002). An analytical–numerical approach to the hydraulics of floating debris in river channels. *Journal of Hydrology*, *269*(1–2), 65–78.

Böhm, R., Auer, I., Brunetti, M., Maugeri, M., Nanni, T., & Schöner, W. (2001). Regional temperature variability in the European Alps: 1760–1998 from homogenized instrumental time series. *International Journal of Climatology: A Journal of the Royal Meteorological Society*, *21*(14), 1779–1801.

Bormann, H., Pinter, N., & Elfert, S. (2011). Hydrological signatures of flood trends on German rivers: Flood frequencies, flood heights and specific stages. *Journal of Hydrology*, *404*(1–2), 50–66.

Brabets, T. P., & Walvoord, M. A. (2009). Trends in streamflow in the Yukon River Basin from 1944 to 2005 and the influence of the Pacific Decadal Oscillation. *Journal of Hydrology*, *371*(1–4), 108–119.

Bradley, A. A. (1998). Regional frequency analysis methods for evaluating changes in hydrologic extremes. *Water Resources Research*, *34*(4), 741–750.

Brázdil, R., Kundzewicz, Z. W., Benito, G., Demarée, G., Macdonald, N., & Roald, L. A. (2012). Historical floods in Europe in the past millennium. *Changes in Flood Risk in Europe, Edited by: Kundzewicz, ZW, IAHS Press, Wallingford*, 121–166.

Brocca, L., Melone, F., & Moramarco, T. (2005). Empirical and conceptual approaches for soil moisture estimation in view of event-based rainfall–runoff modeling. *Progress in Surface and Subsurface Water Studies at the Plot and Small Basin Scale, Edited by: Maraga, F. and Arattano, M., IHP-VI, Technical Documents in Hydrology*, *77*, 1–8.

Brocca, L., Melone, F., Moramarco, T., & Singh, V. P. (2009). Assimilation of observed soil moisture data in storm rainfall-runoff modeling. *Journal of Hydrologic Engineering*, *14*(2), 153–165.

Bronstert, A., & Bárdossy, A. (1999). The role of spatial variability of soil moisture for modelling surface runoff generation at the small catchment scale. *Hydrology and Earth System Sciences*, *3*(4), 505–516.

Brunetti, M., Maugeri, M., & Nanni, T. (2001). Changes in total precipitation, rainy days and

extreme events in northeastern Italy. *International Journal of Climatology: A Journal of the Royal Meteorological Society*, *21*(7), 861–871.

Caloiero, T., Coscarelli, R., Ferrari, E., & Mancini, M. (2011). Trend detection of annual and seasonal rainfall in Calabria (Southern Italy). *International Journal of Climatology*, *31*(1), 44–56.

Chen, C.-J., & Georgakakos, A. P. (2014). Hydro-climatic forecasting using sea surface temperatures: methodology and application for the southeast US. *Climate Dynamics*, *42*, 2955–2982.

Chevuturi, A., Dimri, A. P., & Thayyen, R. J. (2018). Climate change over Leh (Ladakh), India. *Theoretical and Applied Climatology*, *131*, 531–545.

Dallan, E., Borga, M., Zaramella, M., & Marra, F. (2022). Enhanced summer convection explains observed trends in extreme subdaily precipitation in the eastern Italian Alps. *Geophysical Research Letters*, *49*(5), e2021GL096727.

Darand, M., Masoodian, A., Nazaripour, H., & Mansouri Daneshvar, M. R. (2015). Spatial and temporal trend analysis of temperature extremes based on Iranian climatic database (1962–2004). *Arabian Journal of Geosciences*, *8*, 8469–8480.

Day, C. A. (2009). Modelling impacts of climate change on snowmelt runoff generation and streamflow across western US mountain basins: a review of techniques and applications for water resource management. *Progress in Physical Geography*, *33*(5), 614–633.

De Michele, C., Montanari, A., & Rosso, R. (1998). The effects of non-stationarity on the evaluation of critical design storms. *Water Science and Technology*, *37*(11), 187–193.

Di Marco, N., Righetti, M., Avesani, D., Zaramella, M., Notarnicola, C., & Borga, M. (2020). Comparison of MODIS and model-derived snow-covered areas: Impact of land use and solar illumination conditions. *Geosciences*, *10*(4), 134.

Diop, L., Yaseen, Z. M., Bodian, A., Djaman, K., & Brown, L. (2018). Trend analysis of streamflow with different time scales: a case study of the upper Senegal River. *ISH Journal of Hydraulic Engineering*, *24*(1), 105–114.

Douglas, E. M., Vogel, R. M., & Kroll, C. N. (2000). Trends in floods and low flows in the United States: impact of spatial correlation. *Journal of Hydrology*, *240*(1–2), 90–105.

Gafurov, A., & Bárdossy, A. (2009). Cloud removal methodology from MODIS snow cover product. *Hydrology and Earth System Sciences*, *13*(7), 1361–1373.

Gelmini, Y., Zuecco, G., Zaramella, M., Penna, D., & Borga, M. (2022). Hysteresis in streamflow-water table relation provides a new classification system of rainfall-runoff events. *Hydrological Processes*, *36*(9), e14685.

Gocic, M., & Trajkovic, S. (2013). Analysis of changes in meteorological variables using Mann-Kendall and Sen's slope estimator statistical tests in Serbia. *Global and Planetary Change*, *100*, 172–182.

Gregersen, I. B., Madsen, H., Rosbjerg, D., & Arnbjerg-Nielsen, K. (2013). A spatial and

nonstationary model for the frequency of extreme rainfall events. *Water Resources Research*, *49*(1), 127–136.

Guastini, E., Zuecco, G., Errico, A., Castelli, G., Bresci, E., Preti, F., & Penna, D. (2019). How does streamflow response vary with spatial scale? Analysis of controls in three nested Alpine catchments. *Journal of Hydrology*, *570*, 705–718.

Hirsch, R. M., Helsel, D. R., Cohn, T. A., Gilroy, E. J., & Maidment, D. R. (1993). Handbook of hydrology. *Statistical Analysis of Hydrologic Data*.

James, A. L., & Roulet, N. T. (2009). Antecedent moisture conditions and catchment morphology as controls on spatial patterns of runoff generation in small forest catchments. *Journal of Hydrology*, *377*(3–4), 351–366.

Jurko, M., Kobold, M., & Mikoš, M. (2009). Statistical Analysis of Streamflow Trends in Slovenia. *EGU General Assembly Conference Abstracts*, 2001.

Kendall, M. G. (1975). Rank Correlation Methods, Charles Griffin, London (1975). *Google Sch*.

Kliment, Z., Matouskova, M., Ledvinka, O., & Královec, V. (2011). Trend analysis of rainfall-runoff regimes in selected headwater areas of the Czech Republic. *Journal of Hydrology and Hydromechanics*, *59*(1), 36.

Korhonen, J., & Kuusisto, E. (2010). Long-term changes in the discharge regime in Finland. *Hydrology Research*, *41*(3–4), 253–268.

Kundzewicz, Z. W., & Robson, A. J. (2004). Change detection in hydrological records—a review of the methodology/revue méthodologique de la détection de changements dans les chroniques hydrologiques. *Hydrological Sciences Journal*, *49*(1), 7–19.

Kyselý, J. (2009). Trends in heavy precipitation in the Czech Republic over 1961–2005. *International Journal of Climatology: A Journal of the Royal Meteorological Society*, *29*(12), 1745–1758.

Libertino, A., Ganora, D., & Claps, P. (2019). Evidence for increasing rainfall extremes remains elusive at large spatial scales: The case of Italy. *Geophysical Research Letters*, *46*(13), 7437–7446.

Miscel, M. (2023). Analysis of Hydrometeorological Trends in the Cordevole River at La Vizza

Madsen, H., Arnbjerg-Nielsen, K., & Mikkelsen, P. S. (2009). Update of regional intensity–duration–frequency curves in Denmark: Tendency towards increased storm intensities. *Atmospheric Research*, *92*(3), 343–349.

Madsen, H., Lawrence, D., Lang, M., Martinkova, M., & Kjeldsen, T. R. (2014). Review of trend analysis and climate change projections of extreme precipitation and floods in Europe. *Journal of Hydrology*, *519*, 3634–3650.

Mann, H. B. (1945). Nonparametric tests against trend. *Econometrica: Journal of the Econometric Society*, 245–259.

Massari, C., Brocca, L., Moramarco, T., Tramblay, Y., & Lescot, J.-F. D. (2014). Potential of soil moisture observations in flood modelling: Estimating initial conditions and correcting

rainfall. *Advances in Water Resources*, *74*, 44–53.

Meilutytė-Barauskienė, D., Kriaučiūnienė, J., & Kovalenkovienė, M. (2010). Impact of Climate Change on Runoff of the Lithuanian Rivers: Modern Climate Change Models, Statistical Methods and Hydrological Modelling. *Saarbrücken, Germany: LAP LAMBERT Academic Publishing*, 55.

Merz, R., & Blöschl, G. (2009). A regional analysis of event runoff coefficients with respect to climate and catchment characteristics in Austria. *Water Resources Research*, *45*(1).

Mölg, N., Rastner, P., & Irsara, L. (n.d.). *Thomas Schellenberger, Claudia Notarnicola Christian Steurer b Physical Geography Division, Department of Geography, University of Zurich-Switzerland*.

Montanari, A., Rosso, R., & Taqqu, M. S. (1996). Some long-run properties of rainfall records in Italy. *Journal of Geophysical Research: Atmospheres*, *101*(D23), 29431–29438.

Moore, R. J. (2007). The PDM rainfall-runoff model. *Hydrology and Earth System Sciences*, *11*(1), 483–499.

Moraga, J. S., Peleg, N., Fatichi, S., Molnar, P., & Burlando, P. (2021). Revealing the impacts of climate change on mountainous catchments through high-resolution modelling. *Journal of Hydrology*, *603*, 126806.

Musselman, K. N., Clark, M. P., Liu, C., Ikeda, K., & Rasmussen, R. (2017). Slower snowmelt in a warmer world. *Nature Climate Change*, *7*(3), 214–219.

Nash, J. E., & Sutcliffe, J. V. (1970). River flow forecasting through conceptual models part I—A discussion of principles. *Journal of Hydrology*, *10*(3), 282–290.

Norbiato, D., Borga, M., Degli Esposti, S., Gaume, E., & Anquetin, S. (2008). Flash flood warning based on rainfall thresholds and soil moisture conditions: An assessment for gauged and ungauged basins. *Journal of Hydrology*, *362*(3–4), 274–290.

Notarnicola, C., Duguay, M., Moelg, N., Schellenberger, T., Tetzlaff, A., Monsorno, R., Costa, A., Steurer, C., & Zebisch, M. (2013a). Snow cover maps from MODIS images at 250 m resolution, Part 1: Algorithm description. *Remote Sensing*, *5*(1), 110–126.

Notarnicola, C., Duguay, M., Moelg, N., Schellenberger, T., Tetzlaff, A., Monsorno, R., Costa, A., Steurer, C., & Zebisch, M. (2013b). Snow cover maps from MODIS images at 250 m resolution, part 2: Validation. *Remote Sensing*, *5*(4), 1568–1587.

Penna, D., Tromp-van Meerveld, H. J., Gobbi, A., Borga, M., & Dalla Fontana, G. (2011). The influence of soil moisture on threshold runoff generation processes in an alpine headwater catchment. *Hydrology and Earth System Sciences*, *15*(3), 689–702.

Penna, D., van Meerveld, H. J., Zuecco, G., Dalla Fontana, G., & Borga, M. (2016). Hydrological response of an Alpine catchment to rainfall and snowmelt events. *Journal of Hydrology*, *537*, 382–397.

Penna, D., Zuecco, G., Crema, S., Trevisani, S., Cavalli, M., Pianezzola, L., Marchi, L., & Borga, M. (2017). Response time and water origin in a steep nested catchment in the Italian

Dolomites. *Hydrological Processes*, *31*(4), 768–782.

Petrow, T., & Merz, B. (2009). Trends in flood magnitude, frequency and seasonality in Germany in the period 1951–2002. *Journal of Hydrology*, *371*(1–4), 129–141.

Petrow, T., Zimmer, J., & Merz, B. (2009). Changes in the flood hazard in Germany through changing frequency and persistence of circulation patterns. *Natural Hazards and Earth System Sciences*, *9*(4), 1409–1423.

Radatz, T. F., Thompson, A. M., & Madison, F. W. (2013). Soil moisture and rainfall intensity thresholds for runoff generation in southwestern Wisconsin agricultural watersheds. *Hydrological Processes*, *27*(25), 3521–3534.

Sa'adi, Z., Shahid, S., Ismail, T., Chung, E.-S., & Wang, X.-J. (2019). Trends analysis of rainfall and rainfall extremes in Sarawak, Malaysia using modified Mann–Kendall test. *Meteorology and Atmospheric Physics*, *131*, 263–277.

Sadri, S., Madsen, H., Mikkelsen, P. S., & Burn, D. H. (2009). Analysis of extreme rainfall trends in Denmark. *Proceedings of the 33rd IAHR Congress: Water Engineering for a Sustainable Environment*, 1731–1738.

Salas, J. D., & Maidment, D. (1993). Handbook of hydrology. *Analysis and Modeling of Hydrologic Time Series; McGraw-Hill Book Co.: New York, NY, USA*.

Sen, P. K. (1968). Estimates of the regression coefficient based on Kendall's tau. *Journal of the American Statistical Association*, *63*(324), 1379–1389.

Soltani, M., Rousta, I., & Taheri, S. S. M. (2013). Using Mann-Kendall and time series techniques for statistical analysis of long-term precipitation in Gorgan weather station. *World Applied Sciences Journal*, *28*(7), 902–908.

Somers, L. D., & McKenzie, J. M. (2020). A review of groundwater in high mountain environments. *Wiley Interdisciplinary Reviews: Water*, *7*(6), e1475.

Tayfur, G., Zucco, G., Brocca, L., & Moramarco, T. (2014). Coupling soil moisture and precipitation observations for predicting hourly runoff at small catchment scale. *Journal of Hydrology*, *510*, 363–371.

Tramblay, Y., Bouvier, C., Martin, C., Didon-Lescot, J.-F., Todorovik, D., & Domergue, J.-M. (2010). Assessment of initial soil moisture conditions for event-based rainfall–runoff modelling. *Journal of Hydrology*, *387*(3–4), 176–187.

Uber, M., Vandervaere, J.-P., Zin, I., Braud, I., Heistermann, M., Legoût, C., Molinié, G., & Nord, G. (2018). How does initial soil moisture influence the hydrological response? A case study from southern France. *Hydrology and Earth System Sciences*, *22*(12), 6127–6146.

Umar, S., Lone, M. A., Goel, N. K., & Zakwan, M. (2022). Trend analysis of hydro-meteorological parameters in the Jhelum River basin, North Western Himalayas. *Theoretical and Applied Climatology*, *148*(3–4), 1417–1428.

Wang, X., & Xie, H. (2009). New methods for studying the spatiotemporal variation of snow cover based on combination products of MODIS Terra and Aqua. *Journal of Hydrology*, *371*(1–4),

192–200.

Western, A. W., Zhou, S.-L., Grayson, R. B., McMahon, T. A., Blöschl, G., & Wilson, D. J. (2004). Spatial correlation of soil moisture in small catchments and its relationship to dominant spatial hydrological processes. *Journal of Hydrology*, *286*(1–4), 113–134.

Wilson, D., Hisdal, H., & Lawrence, D. (2010). Has streamflow changed in the Nordic countries?–Recent trends and comparisons to hydrological projections. *Journal of Hydrology*, *394*(3–4), 334–346.

Wu, H., & Qian, H. (2017). Innovative trend analysis of annual and seasonal rainfall and extreme values in Shaanxi, China, since the 1950s. *International Journal of Climatology*, *37*(5), 2582–2592.

Zaramella, M., Borga, M., Zoccatelli, D., & Carturan, L. (2019). TOPMELT 1.0: a topography-based distribution function approach to snowmelt simulation for hydrological modelling at basin scale. *Geoscientific Model Development*, *12*(12), 5251–5265.

Zehe, E., Becker, R., Bárdossy, A., & Plate, E. (2005). Uncertainty of simulated catchment runoff response in the presence of threshold processes: Role of initial soil moisture and precipitation. *Journal of Hydrology*, *315*(1–4), 183–202.

Zehe, E., & Blöschl, G. (2004). Predictability of hydrologic response at the plot and catchment scales: Role of initial conditions. *Water Resources Research*, *40*(10).

Zehe, E., Graeff, T., Morgner, M., Bauer, A., & Bronstert, A. (2010). Plot and field scale soil moisture dynamics and subsurface wetness control on runoff generation in a headwater in the Ore Mountains. *Hydrology and Earth System Sciences*, *14*(6), 873–889.

Zhao, N., Yu, F., Li, C., Zhang, L., Liu, J., Mu, W., & Wang, H. (2015). Soil moisture dynamics and effects on runoff generation at small hillslope scale. *Journal of Hydrologic Engineering*, *20*(7), 5014024.

Zuecco, G., Penna, D., & Borga, M. (2018). Runoff generation in mountain catchments: long-term hydrological monitoring in the Rio Vauz Catchment, Italy. *Cuadernos de Investigación Geográfica: Geographical Research Letters*, *44*, 397–428.

Appendix

Annex 1: Statistics for annual maxima of rainfall. * indicate statistically significant trend at level of significance (α)= 0.05

Weather Station	Stat	Max_5min	Max_10min	Max_15min	Max_30min	Max_45min	Max_1h	Max_3h	Max_6h	Max_12h	Max_24h
Arabba	Sen_slope_1d	0.00018	0.00027	0.00043	0.00064	0.00062	0.00057	0.00074	0.00037	0.00034	0.00000
	p_value	**0.04** *	**0.04** *	**0.01** *	**0.00** *	**0.01** *	**0.01** *	**0.00** *	0.31	0.65	0.99
	Mean	5.80	9.07	11.37	15.34	17.74	19.27	29.75	41.87	60.66	77.21
	Sen_10y	0.67	1.00	1.55	2.33	2.27	2.08	2.71	1.33	1.23	0.00
	Sen_10y_perc (%)	11.49	11.02	13.67	15.20	12.77	10.77	9.12	3.18	2.03	0.00
Caprile	Sen_slope_1d	0.00003	0.00008	0.00015	0.00027	0.00035	0.00028	0.00027	0.00008	-0.00021	0.00004
	p_value	0.59	0.54	0.39	0.29	0.22	0.30	0.24	0.90	0.57	0.98
	Mean	6.48	10.25	12.67	16.52	18.32	19.76	30.56	42.59	60.36	79.30
	Sen_10y	0.12	0.29	0.53	1.00	1.29	1.04	1.00	0.30	-0.75	0.13
	Sen_10y_perc (%)	1.93	2.78	4.21	6.05	7.06	5.24	3.27	0.70	-1.24	0.17
Biois a Cencenighe	Sen_slope_1d	0.00013	0.00025	0.00011	-0.00005	-0.00004	-0.00025	-0.00053	-0.00185	-0.00160	-0.00175
	p_value	0.31	0.40	0.76	0.87	0.94	0.53	0.59	0.34	0.51	0.69
	Mean	6.16	9.68	11.42	14.93	18.34	20.48	38.43	60.62	90.46	120.79
	Sen_10y	0.47	0.90	0.40	-0.18	-0.14	-0.91	-1.94	-6.74	-5.83	-6.38
	Sen_10y_perc (%)	7.66	9.28	3.50	-1.18	-0.78	-4.45	-5.05	-11.12	-6.44	-5.29
Falcade	Sen_slope_1d	0.00013	0.00025	0.00011	-0.00005	-0.00004	-0.00025	-0.00053	-0.00185	-0.00160	-0.00175
	p_value	0.31	0.40	0.76	0.87	0.94	0.53	0.59	0.34	0.51	0.69
	Mean	6.16	9.68	11.42	14.93	18.34	20.48	38.43	60.62	90.46	120.79
	Sen_10y	0.47	0.90	0.40	-0.18	-0.14	-0.91	-1.94	-6.74	-5.83	-6.38
	Sen_10y_perc (%)	7.66	9.28	3.50	-1.18	-0.78	-4.45	-5.05	-11.12	-6.44	-5.29
Malga Ciapela	Sen_slope_1d	0.00018	0.00024	0.00024	0.00026	0.00032	0.00033	0.00039	0.00059	0.00058	0.00025
	p_value	**0.02** *	0.10	0.16	0.27	0.21	0.20	0.17	0.15	0.50	0.81
	Mean	5.98	9.34	11.59	15.68	18.21	20.18	31.14	44.09	65.16	87.08
	Sen_10y	0.67	0.88	0.86	0.97	1.16	1.21	1.44	2.16	2.12	0.90
	Sen_10y_perc (%)	11.14	9.46	7.43	6.16	6.38	5.98	4.63	4.90	3.25	1.03
Passo Falzarego	Sen_slope_1d	0.00018	0.00024	0.00024	0.00026	0.00032	0.00033	0.00039	0.00059	0.00058	0.00025
	p_value	**0.02** *	0.10	0.16	0.27	0.21	0.20	0.17	0.15	0.50	0.81
	Mean	5.98	9.34	11.59	15.68	18.21	20.18	31.14	44.09	65.16	87.08
	Sen_10y	0.67	0.88	0.86	0.97	1.16	1.21	1.44	2.16	2.12	0.90
	Sen_10y_perc (%)	11.14	9.46	7.43	6.16	6.38	5.98	4.63	4.90	3.25	1.03
Passo Pordoi	Sen_slope_1d	0.00008	0.00018	0.00026	0.00050	0.00061	0.00062	0.00059	0.00033	-0.00023	-0.00043
	p_value	0.26	0.11	**0.05** *	**0.01** *	**0.00** *	**0.01** *	0.07	0.33	0.63	0.54
	Mean	5.62	8.92	11.14	15.82	18.67	20.49	30.43	38.77	48.89	59.99
	Sen_10y	0.29	0.65	0.93	1.83	2.23	2.25	2.15	1.20	-0.84	-1.57
	Sen_10y_perc (%)	5.08	7.25	8.37	11.58	11.97	10.97	7.07	3.09	-1.72	-2.62
Passo Valles	Sen_slope_1d	0.00008	0.00018	0.00026	0.00050	0.00061	0.00062	0.00059	0.00033	-0.00023	-0.00043
	p_value	0.26	0.11	**0.05** *	**0.01** *	**0.00** *	**0.01** *	0.07	0.33	0.63	0.54
	Mean	5.62	8.92	11.14	15.82	18.67	20.49	30.43	38.77	48.89	59.99
	Sen_10y	0.29	0.65	0.93	1.83	2.23	2.25	2.15	1.20	-0.84	-1.57
	Sen_10y_perc (%)	5.08	7.25	8.37	11.58	11.97	10.97	7.07	3.09	-1.72	-2.62
Pescul	Sen_slope_1d	0.00008	0.00018	0.00026	0.00050	0.00061	0.00062	0.00059	0.00033	-0.00023	-0.00043
	p_value	0.26	0.11	**0.05** *	**0.01** *	**0.00** *	**0.01** *	0.07	0.33	0.63	0.54
	Mean	5.62	8.92	11.14	15.82	18.67	20.49	30.43	38.77	48.89	59.99
	Sen_10y	0.29	0.65	0.93	1.83	2.23	2.25	2.15	1.20	-0.84	-1.57
	Sen_10y_perc (%)	5.08	7.25	8.37	11.58	11.97	10.97	7.07	3.09	-1.72	-2.62
Selva di Cadore	Sen_slope_1d	0.00008	0.00018	0.00026	0.00050	0.00061	0.00062	0.00059	0.00033	-0.00023	-0.00043
	p_value	0.26	0.11	**0.05** *	**0.01** *	**0.00** *	**0.01** *	0.07	0.33	0.63	0.54
	Mean	5.62	8.92	11.14	15.82	18.67	20.49	30.43	38.77	48.89	59.99
	Sen_10y	0.29	0.65	0.93	1.83	2.23	2.25	2.15	1.20	-0.84	-1.57
	Sen_10y_perc (%)	5.08	7.25	8.37	11.58	11.97	10.97	7.07	3.09	-1.72	-2.62

Annex 2: Statistics for mean annual temperature. * indicate statistically significant trend at level of significance (α)= 0.05

Statistics→ Weather Station↓	Sen_slope_1d	p_value (at α= 0.05)	Min	Mean	Max	St_dev	Sen_10y	Change in Sen_10y (%)
Pian Fedaia	0.000103	**0.0156 ***	1.3371	2.7062	3.9008	0.6298	0.3752	13.8653
Arabba	0.000171	**0.0301 ***	3.9292	5.0724	6.3271	0.6166	0.6258	12.3371
Passo Pordoi	0.000130	**0.0424 ***	0.8423	2.4439	3.4832	0.6611	0.4734	19.3682

Annex 3: Statistics for antecedent SWE. * indicate statistically significant trend at level of significance (α)= 0.05

Statistics→ Timescale↓	Sen_slope_1d	p_value (at α= 0.05)	Min	Mean	Max	St_dev	Sen_10y	Change in Sen_10y (%)
Annual	-5.02E-06	**6.53E-16 ***	0.000	30.706	1046.558	89.522	-0.018	-0.060
Winter	6.76E-03	5.36E-01	20.808	106.144	207.065	62.753	24.679	23.251
Spring	-4.97E-03	**2.14E-05 ***	0.000	74.207	1011.814	103.959	-18.150	-24.459
Summer	0.00E+00	**1.26E-11 ***	0.000	23.792	1046.558	92.371	0.000	0.000
Autumn	-6.78E-06	**4.43E-02 ***	0.000	11.360	410.323	43.275	-0.025	-0.218

Annex 4: Statistics for antecedent SM. * indicate statistically significant trend at level of significance (α)= 0.05

Statistics→ Timescale↓	Sen_slope_1d	p_value (at α= 0.05)	Min	Mean	Max	St_dev	Sen_10y	Change in Sen_10y (%)
Annual	-1.65E-07	0.844	0.281	0.697	1.000	0.108	-0.001	-0.086
Winter	7.68E-06	0.108	0.453	0.488	0.563	0.037	0.028	5.736
Spring	-5.00E-06	0.084	0.281	0.695	1.000	0.127	-0.018	-2.628
Summer	1.22E-06	0.277	0.479	0.714	1.000	0.102	0.004	0.625
Autumn	6.43E-07	0.752	0.394	0.656	1.000	0.089	0.002	0.358

Annex 5: Statistics for event characteristics. * indicate statistically significant trend at level of significance (α)= 0.05

Statistics→ Event Characteristics↓	**Sen_slope_1d**	**p_value (at α= 0.05)**	**Min**	**Mean**	**Max**	**St_dev**	**Change in Sen_10y (%)**
Cumulative Precipitation	0.0002	**0.009 ***	1.800	22.614	342.400	26.433	3.620
Average Rainfall Intensity	2.75E-05	**0.00 ***	0.325	2.084	12.467	1.420	4.814
Q_{max} (Streamflow Peak)	-4.90E-06	**0.07 ***	0.070	0.639	3.980	0.519	-2.798
RC (Runoff Ratio)	-8.81E-07	**0.05 ***	0.001	0.091	0.989	0.113	-3.536

Annex 6: Acronyms

ARPAV	Agenzia Regionale per la Prevenzione e Protezione Ambentale del Veneto
AM	Annual Maxima
DTM	Digital Terrain Model
EURAC	Réseau Européen pour l'Afrique Centrale
GIS:	Geographic Information System
IPCC	Intergovernmental Panel on Climate Change
MODIS	Moderate Resolution Imaging Spectroradiometer
min	Minute
mm	Millimetre
NSE	Nash Sutcliff Efficiency
PDM	Probability Distributed Model
Q	Runoff
SCA	Snow Cover Area
SM	Soil Moisture
SWE	Snow Water Equivalent
y	Year